MONITORING PROTIEN CAGE NANOPATICLE MORPHOLOGY FOR APPLICATIONS IN MEDICINES AND MATERIALS

by

Benjamin Lawrence Johnson

A thesis submitted in partial fulfillment
of the requirements for the degree

of

Master of Science

in

Biochemistry

MONTANA STATE UNIVERSITY
Bozeman, Montana

April 2011

©COPYRIGHT

by

Benjamin Lawrence Johnson

2011

All Rights Reserved

APPROVAL

of a thesis submitted by

Benjamin Lawrence Johnson

This thesis has been read by each member of the thesis committee and has been found to be satisfactory regarding content, English usage, format, citation, bibliographic style, and consistency and is ready for submission to The Graduate School.

Dr. Trevor Douglas

Approved for the Department of Chemistry and Biochemistry

Dr. David Singel

Approved for The Graduate School

Dr. Carl A. Fox

STATEMENT OF PERMISSION TO USE

In presenting this thesis in partial fulfillment of the requirements for a master's degree at Montana State University, I agree that the Library shall make it available to borrowers under rules of the Library.

If I have indicated my intention to copyright this thesis by including a copyright notice page, copying is allowable only for scholarly purposes, consistent with "fair use" as prescribed in the U.S. Copyright Law. Requests for permission for extended quotation from or reproduction of this thesis in whole or in parts may be granted only by the copyright holder.

Benjamin Lawrence Johnson

April 2011

ACKNOWLEDGEMENTS

I would like to thank Dr. Trevor Douglas for aiding me in my growth as a scientist and always providing the facilities and tools that I needed to grow. I would also like to thank my mother for reading my thesis and providing excellent feedback and being there when I needed the support. Also, thank you to Chris Broomell for reading and editing my thesis and providing excellent feedback. Most importantly, thank you to Melinda for always being there for me and supporting me through this.

TABLE OF CONTENTS

1. PROTEIN CAGE NANOPARTICLES AS MATERIALS: A LOOK AT THE HISTORY OF BIOLOGICALLY PRODUCED PROTEINCAGES AND THEIR USE IN MATERIALSYNTHESIS 1

Protein cage nanoparticles 1
sHsp from *Methanococcus jannaschii* 3
Structure and Function 3
sHsp Use In Nano-technology 6
Bacteriophage P22 8
Structure and Assembly 8
P22 As A Platform For Nano-technology 14
Other PCN 16
Cowpea Chlorotic Mottle Virus 16
Human Ferritin 18
DNA Binding Protein From Starved Cells 20
Dendrimer 20
Other PCN Not Covered In This Thesis 21
Instrumentation 22
Size Exclusion Chromatography 22
Multi Angle Static Light Scattering 23
Dynamic light scattering 24
Analytical Ultra Centrifugation 25

2. MONITORING THE STRUCTURAL TRANSITIONS IN THE BACTERIOPHAGE P22 26

Introduction 26
Results and Discussion 27
Results 27
Binding Of OmpF To The P22 Capsid 27
Two Distinct Morphologies Are Present When P22 Is Heated To 75°C 32
Photo Cross-linking Has Different Stabilizing Effect In The Presence Of OmpF 36
pH Stability 37
Discussion 39
Two Distinct Morphologies Are Present When P22 Is Heated To 75°C 39
Binding Of OmpF To The P22 capsid 41
pH Stability 42
Photo Cross-linking Has Different Stabilizing Effect In The Presence Of OmpF 43

TABLE OF CONTENTS – CONTINUED

Conclusions 44

3.UNDERSTANDING THE MECHANISM FOR THE PRODUCTION OF INDUCED BRONCHIAL ASSOCIATED LYMPHOID TISSUE WITH PROTEIN CAGE NANOPARTICLES 46

iBALT-Structure And Function 46
Destabilizing The sHsp Cage 52
Induction Of iBALT With Different PCN 57
Dose Response Studies 63
Testing For iBALT Response In Other Animal Models 66
Conclusions 68

REFERENCES CITED 70

APPENDICES 87

APPENDIX A: MATERIALS AND METHODS 87

LIST OF FIGURES

Figure Page

1.1 Protein cage library 1

1.2 Surfaces of a protein cage 2

1.3 Image of *Methanococcus jannaschii* 4

1.4 Structure of small heat shock protein form *M. jannaschii* 5

1.5 *Salmonella typhimurium* 9

1.6 Life cycle of P22 10

1.7 Bacteriophage P22 11

1.8 Different morphological states of P22 12

1.9 Conformations of CCMV 16

1.10 Structure of Human Ferritin 18

2.1 P22 purification 28

2.2 P22 SDS-PAGE 28

2.3 DLS of multiple forms of P22 29

2.4 SEC-MALS multiple forms of P22 30

2.5 Native gel of multiple forms of P22 32

2.6 SDS-PAGE of OmpF association while heating 33

2.7 AUC of multiple forms of P22 34

2.8 TEM of WB 34

LIST OF FIGURES - CONTINUED

Figure Page

2.9 Chromatogram of lipid 255.31 Da 35

2.10 90° SLS of cross-linked P22 36

2.11 Transitions in P22 at different pH 37

2.12 SEC-MALS transition in P22 at different pH 39

2.13 TEM of different morphologies 40

2.14 Native gel of P22 heated to 75 40

2.15 SDS-PAGE binding of OmpF 41

3.1 iBALT structure 47

3.2 Histology from mice treated with HFn 51

3.3 Mice treated wit different proteins 51

3.4 Destabilizing mutations made in sHsp 53

3.5 R93E subunit mass 54

3.6 Assembly of R93E into a cage 54

3.7 90° static scattering of G41C 55

3.8 90° SLS of multiple cages 56

3.9 CD of G41C 56

3.10 PCN used in mice 57

3.11 Percent weight loss for mice given multiple PCN 59

3.12 Viral recovery from mice given multiple PCN 59

LIST OF FIGURES - CONTINUED

Figure Page

3.13 Influenza specific antibodies in mice given multiple PCN 60

3.14 Histology for mice given multiple PCN 62

3.15 Percent weight lose for mice with differing amounts of sHsp 64

3.16 Viral recovery for mice treated with different amounts of sHsp 64

3.17 Histology for mice treated with differing amounts of sHsp 65

3.18 Histology for ferrets treated with sHsp 67

3.19 Percent weight loss in ferrets treated with sHsp 68

LIST OF TABLES

Table Page

3.1 Number of particles delivered 57

ABSTRACT

Protein cage nanoparticles are naturally occurring proteins found in all domains of life. The breadth of structural knowledge and the ability to modify protein cage nanoparticles both chemically and genetically set them apart for use as platforms for biomedical templates and materials synthesis. The work described herein focuses on the use of protein cage nanoparticles as a protective agent from a suite of viral pathogens. Protein cage nanoparticles exist in many different morphological forms both within a specific particle and between particles. It is essential to characterize these different states in order to engineer a protein cage nano particle for biomedical and materials synthesis.

Described here is an expanded protocol for determining the morphological state with the bacteriophage P22 capsid. Using multiple techniques including multi angle light scattering, analytical ultra centrifugation, agarose gel electrophoresis and transmission electron microscopy these states are described and characterized. P22 exits in four different morphological states: the procapsid, empty shell, expanded shell and so-called “wiffleball”. Also characterized in the work is the small heat shock protein from *Methanococcus jannaschii,* which exists in two morphological states. One of the states being the assembled 12 nm cage structure and the other state being a disassembled cage structure that is most commonly described at elevated temperatures. The characterization of these structures can aid in the understanding the mechanism of formation for the immunological phenomena induced bronchial associated lymphoid tissue.

CHAPTER 1

PROTEIN CAGE NANOPARTICLES AS MATERIALS: A LOOK AT THE HISTORY OF BILOGICALLY PRODUCED PROTEIN CAGES AND THEIR USE IN MATERIALSYNTHESIS

Protein Cage Nanoparticles

Nanobiotechnology is the study of nano-sized biomolecules for use as materials. One of the more promising biomolecules being researched is protein cage nanoparticles (PCN). PCN are naturally occurring particles that exist in all domains of life, bacteria, archea and eukaryotes. These particles self-assemble into hollow cage-like structures. PCN have a diverse range of function from the structural proteins of viruses to ferritins to heat shock proteins and enzyme assemblies (figure 1.1). PCN can be found within and/or infecting organisms that inhabit extreme chemical environments including high salt, extreme pH and extreme temperatures [4-19]. Viruses have shown a remarkable ability to

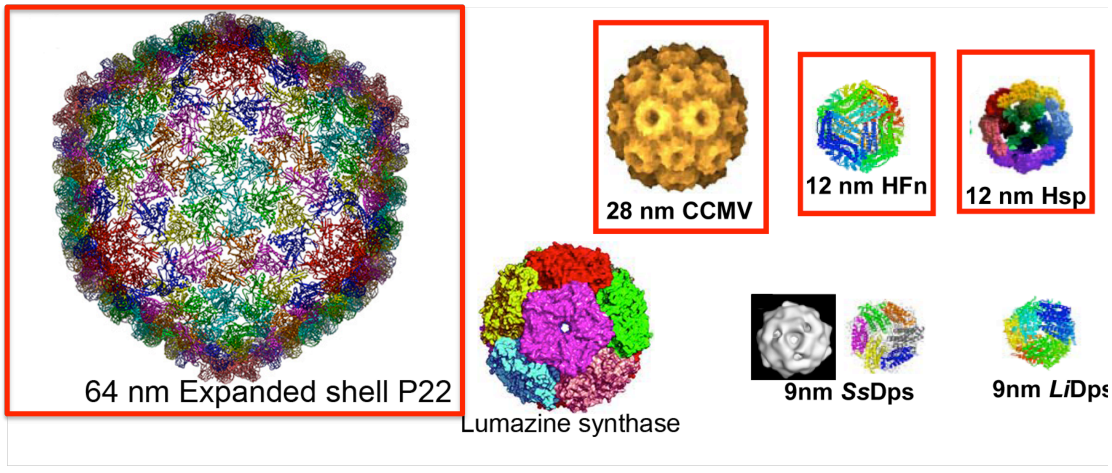


Figure 1.1: Protein cage library.
Space filling models of some protein cages that have been used in materials synthesis. From left to right P22[24], Lumazine synthase[26], CCMV[21], SsDps[51], HFn[23], sHsp[20], LiDps[53]. The red box indicates those cages that were used in this thesis.

“survive” in these extreme environments and still maintain their ability for site-specific delivery of their cargo [4]. While other PCN are produced by the organism in these extreme environments and perform a variety of functions that aid in the survival of those organisms. The use of PCN from extreme conditions provide an ultra stable platform for genetic and chemical manipulation providing a range of different material and medicinal possibilities [27-50]. Encapsulating a cargo, protecting it from degradation and delivering it to a specific location may provide more robust materials for medical and materials science.

Both viral and non-viral (PCN) can be viewed as multifunctional nano-containers [25]. PCN can be both chemically and/or genetically manipulated at

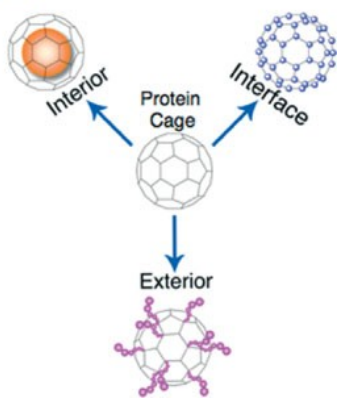


Figure 1.2: Surfaces of a protein cage
Schematic illustration of the three regions of a protein cage available for chemical and genetic modification. Figure from [25]

their exterior surface, the interior surface and the subunit interface (figure 1.2). These regions allow for the attachment of imaging agents or drugs on the interior or subunit interface where they are protected, while also maintaining the ability to

attach a targeting peptide or molecule on the exterior of the cage [35, 41, 43, 44]. It has been demonstrated that labeling a PCN on the exterior can add additional functionality to the PCN. For example Uchida et al. demonstrated that a PCN with a peptide designed to target integrins attached to the outside can aid in the imaging of artherosclerotic plaques by delivering ferrihydrate (an MRI contrast agent) [52]. This targeting mechanism allows for tissue specific delivery of an imagining agent to a tissue thus allowing for an easier diagnosis of a potentially deadly disease [52]. By exploiting PCNs' natural ability to encapsulate and shield molecules, combined with chemical and genetic modifications, the potential for safer and more effective drugs exists.

This thesis describes the characterization of the bacteriophage P22 as a nanoparticles material and explores the effects of specific chemical and genetic modifications to the capsid. Additionally the development of PCN as a specific prophylaxis to respiratory infections is discussed.

sHsp From *Methanococcus jannaschii*

Structure and Function. One of the many cage-like architectures that has been used as a template for nanobiotechnology is the small heat shock protein (sHsp) from *Methanococcus jannaschii* (a hyperthermophile). *M. jannaschii* is a member of the archeon family that was isolated in 1983 from a hydrothermal vent 2,600 meters deep in the Pacific ocean [54] (figure 1.3). Conditions around these vents often reach extremes such as temperatures reaching above 100°C. *M. jannaschii* thrives in extreme conditions including temperatures of 85°C and

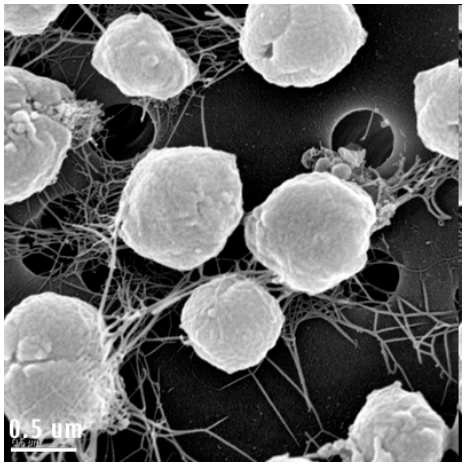


Figure 1.3: Image of *methanocuccus jannaschii*.
M. jannaschii grown at 78°C and 30 psi [3].

pressures upwards of 30psi. Its existence in these extreme conditions has resulted in some of its proteins evolving to withstand extreme conditions on their own. The genome of *Methanococcus jannaschii* was the first archaeal genome sequenced (in 1996) and consists of a 1.6 million base pair circular chromosome and two extra chromosomal units large (58 kbp) and small (16 kbp) [55].

One of the proteins that the *Methanococcus jannaschii* genome encodes for is the sHsp that assembles from 24 identical 16.5 kDa protein subunits forming a cage with cubic (4:3:2) symmetry [20, 56, 57] (figure 1.4). The sHsp crystal structure has been solved to 3.2 Å [20, 56] providing the location of most amino acids. Having a high-resolution structure is critical because it allows for modifications to be made with a predictable effect. Thirty-two residues on the N-termini were not resolved by crystallography, however when observed by cryo-electron microscopy it appears as though these residues reside on the interior of the cage [20, 58]. sHsp has an exterior diameter of 12nm and an interior

diameter of 6.5 nm with 8 3nm pores located at the 3 fold axes (figure 1.4) [20, 56]. These pores allow for the cage to freely exchange bulk solution between the

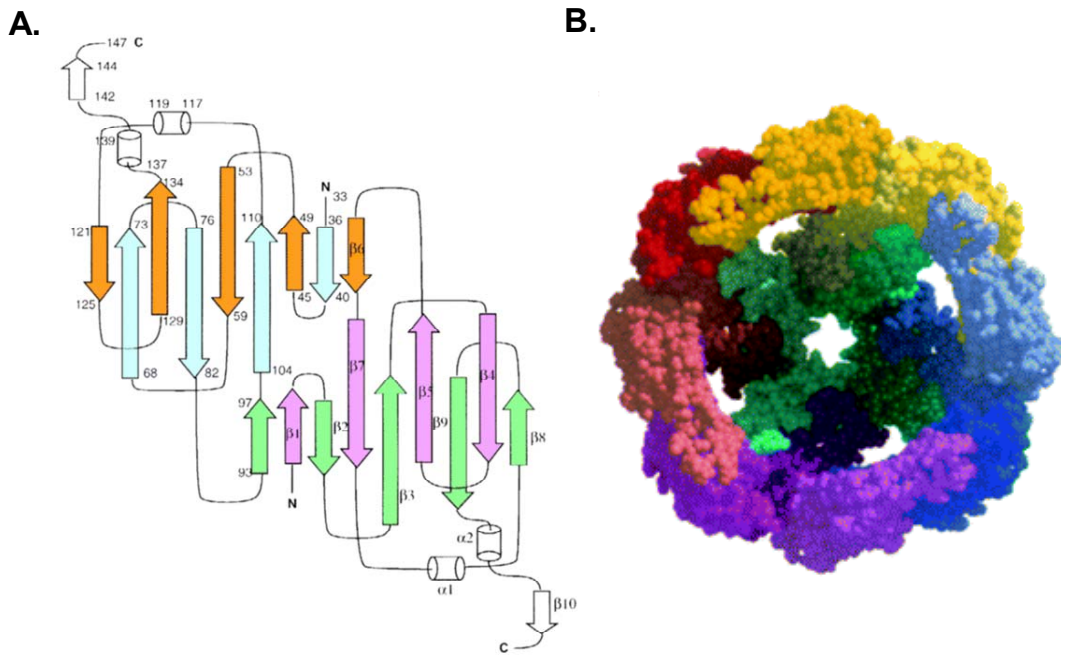


Figure 1.4: Structure of the small heat shock protein from *M. jannaschii*.
A) topology diagram showing the interaction between two of the sHsp subunits. B) Space filling model of the 12nm diameter assembled cage - an interior view along the four-fold axis [20].

interior and the exterior of the cage. Six smaller (1.7nm) pores also exist at the 4-fold axis contributing to the bulk solvent exchange with the interior (figure 1.4) [20, 56, 57]. sHsp is an extremely stable protein remaining stable at temperatures above 90°C and in a pH range of 5 to 11 [59]. The sHsp belongs to the small heat shock protein family HSP-16.5, which can be found in every domain of life [60]. These sHsp function as molecular chaperones that aid in the proper folding of other proteins. All of these heat shock proteins (Hsp) share a common motif; an approximately 100 residue alpha crystalline domain (amino acids 46 to 135 in sHsp) [20, 57]. Alpha crystalline proteins are commonly found

in the eye lens of vertebrates and help to prevent the aggregation of other proteins that may lead to cataract formation. Proteins from this family typically have a subunit size ranging from 12 to 42 KDa [61]. These proteins are typically over expressed during periods stress such as elevated temperatures. Interestingly, heterologously expressed sHsp protects *E. coli* proteins from aggregation when co-expressed *in vitro* but the native *in vivo* function of sHsp in *Methanococcus janaschii* remains unknown [18, 57, 59]. One interesting feature of the sHsp from *Methanococcus janaschii* is that it undergoes subunit exchange at elevated temperatures as shown by fluorescence resonance energy transfer (FRET) [62]. Combined with its stable structure, ease of modification and its high-resolution structure, sHsp is a viable platform for nano-technology research.

sHsp Use In Nanotechnology: The Douglas laboratory has demonstrated the ability to modify the sHsp both chemically and genetically to create many useful platforms and applications for this PCN [38, 63]. G41C is an ideal genetic mutant of sHsp as it provides a unique internally located sulfhydryl group that is accessible for chemical modification. Abedin et al. have recently utilized this site to generate an internally cross-linked sHsp [64]. This was achieved by attachment of an alkyne moiety to the internal cysteine of G41C and subsequent polymerization via the well-characterized [3+2] cyclo-addition ‘click’ chemistry [64]. This polymerization approach allows for diverse chemical functionalities to be introduced to the polymer on the cage interior through an additional side group on the azide cross-linker. By adding these functionalities on the interior of

the cage it should minimize their degradation and shield them from the outside world. For example, Liepold et al. have utilized this system to introduce Gd-DTPA onto the internal polymer [44]. This enhances the “brightness” of the molecule as a T1 MRI contrast agent as compared to Gd-DTPA alone [44]. Another advantage to this method is that it increases the local concentration of Gd thus increasing the potential signal [44].

The sHsp cage has also been used as a potential drug delivery agent. Flenniken et al. showed that doxorubicin (dox), a widely used anti-cancer drug, could be attached to interior of the sHsp G41C cage and subsequently released [35]. A form of dox, (6-maleimidocaproyl) hydrazone of doxorubicin, was attached via malamide to the internal cysteine with near complete labeling of all 24 subunits [35]. This cargo could then be selectively released into the bulk solvent by lowering the pH with a more rapid release as the solution become more acidic [35]. pH-triggered drug release is important because when a molecule is endocytosed into a cell they are engulfed by a structure known as an endosome with a pH range of 3 to 5 [65]. Therefore, if the cage can be targeted to a specific cell and endocytosed, selective destruction of cells could be achieved.

The sHsp protein has been used as a prophylaxis against some viral pathogens in mouse models [66]. In doing toxicity studies it was noticed that sHsp elicited the formation of tertiary lymphoid structures in the lung known as inducible bronchus associated lymphoid tissues (iBALT). These iBALT structures have been shown to enhance immune protection against respiratory pathogens [67]. sHsp delivered intranasally to mice lead to the formation of tertiary lymphoid

structures referred to as induced bronchial associated lymphoid tissue (iBALT). These iBALT structures are rich in B and T-cell [68]. iBALT are typically only associated with respiratory infections (e.g. influenza) [69]. Wiley et al. have shown that these structures can aid in the protection of mice against future respiratory infections [67]. Mice that were dosed with sHsp and subsequently challenged with a lethal dose of influenza did not exhibit the morbidity and mortality characteristic of a viral infection. sHsp-treated mice showed lower viral burdens in their lung and greater influenza specific antibody titers. Interestingly, sHsp was also shown to protect mice from other respiratory viruses including SARS and pneumovirus. These data suggest that sHsp-initiated iBALT can provide a broad range of protection perhaps by priming the immune system to rapidly clear a subsequent viral/pathogen infection [66].

Bacteriophage P22

Structure and Assembly.

P22 is one of the most well studied bacteriophages and is quickly becoming an ideal platform for nanobiotechnology. P22 naturally infects *Salmonella typhimurium* [70] which is a rod shaped, gram-negative enterobacteria that is closely related to the genus *Escherichiai* (figure 1.5). This genus of bacteria is found in both cold-blooded and warm-blooded animals worldwide. P22 begins its infection by binding to the O-antigen, part of the lipopolysaccharides, on the outer membrane by attaching with a portion of its tail-spike [71, 72]. This tail-spike assembly injects the 44 kbp double stranded

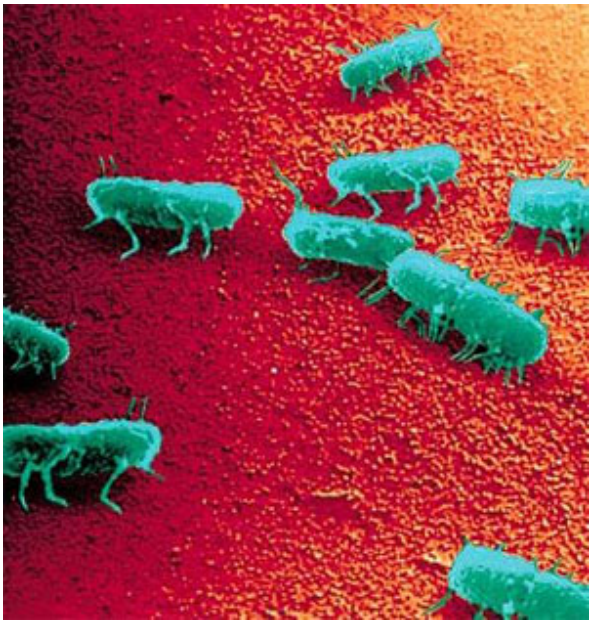


Figure 1.5: *Salmonella typhimurium*
Image showing P22s host *Salmonella typhimurium* [2].

DNA (dsDNA) genome of P22 into the cell where it circularizes and begins to take over host cell machinery [73]. This DNA encodes structural proteins required for phage assembly including the coat protein (CP), the scaffold protein (SP), the portal complex and the tail-spike. Once these proteins begin production 415 copies of the 46.6 kDa CP assemble into a spherical T=7 structure with as many as 300 of 33KDa SP. SP aids in assembly by guiding the CP to ensure the correct assembly of the phage head. The dodecameric portal complex initiates this assembly reaction by allowing the structural proteins to assemble around this complex [72, 74-77] (figure 1.6). The two virally encoded proteins that assemble to form the portal complex package the DNA using ATP [78, 79]. This DNA

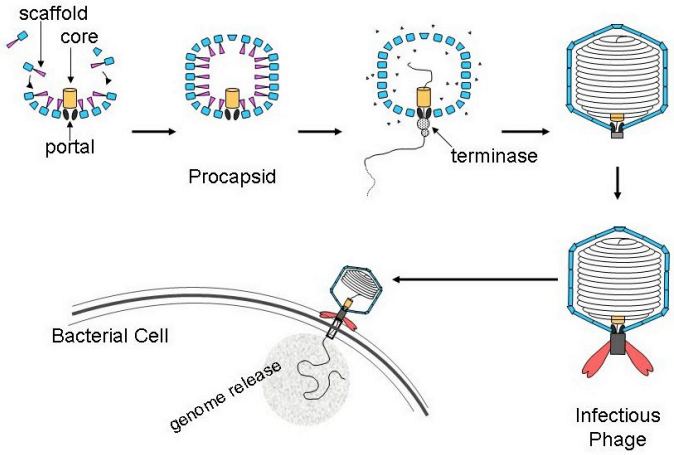


Figure 1.6: Life cycle of P22
An illustration showing the maturation of the bacteriophage P22 from proteins to infectious phage [24].

packaging causes extreme stress on the head structure with internal pressures reaching up to 60atm [80, 81]. As the DNA packaging process begins, all scaffold proteins are released from within the head fully intact. It is hypothesized that the scaffold protein is able to exit through channels that are present at the five-fold axis [79]. The phage head undergoes a dramatic morphological change that includes a large reorganization of the subunit structure as well as a thinning of the protein subunits and is also accompanied by a swelling and structural reorganization of the capsid ultrastructure [74-76] (figure 1.6). It is unknown if the morphological change occurs before the DNA is packaged or if it is a simultaneous process. After the DNA is completely packaged into the head, the portal complex undergoes a dramatic conformational change. This change is thought to be the beginning of the tail-spike formation, a protein complex that is

added to the portal complex which allows for the infectious virus to attach to its host and inject its DNA [77] (figure 1.6). Following this conformational change the injection proteins are recruited and the mature phage conformation is adopted [77] (figure 1.7). After complete maturation the host cell is lysed and the phage are released to propagate infection.

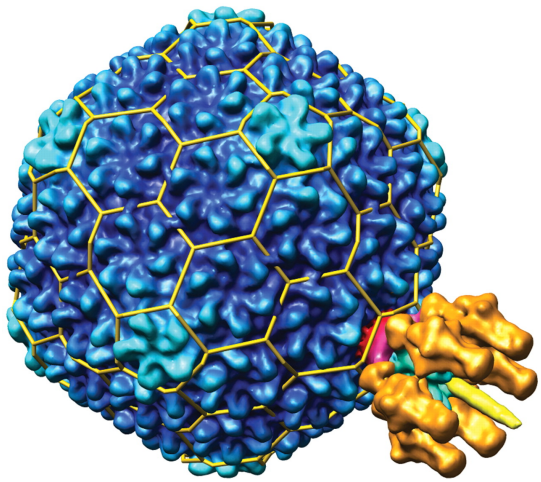


Figure 1.7: Bacteriophage P22
Space filling model of the infective form of a bacteriophage P22 [22].

Bacteriophage P22 has been extensively characterized with respect to the assembly and infection processes as well as its multiple structural configurations [1, 70, 74-76, 82-85]. The P22 head has two major naturally occurring forms. The procapsid (PC) form consists of 415 coat proteins, as many as 300 scaffold proteins and the dodecameric portal complex with an outer diameter of 60nm [74-77, 86]. The majority of the scaffolding protein structure is unknown to date. However, the structure has been determined for amino acids 141 to 303 and it has been established that they are involved in the contact with the CP [87]. SP can form both dimers and tetramers in solution and this process is thought to aid

in directing the CP to the proper location for assembly [86]. Interestingly, the only residues that are required for proper assembly of the PC form are residues 141-303. The second naturally occurring form is the mature phage, which consists of the expanded 64nm head containing 415 copies of the CP, the portal complex and the tail spike [74-77, 86]. The SP has exited the capsid and the DNA has been packaged. The portal complex is 15nm in diameter and 11nm tall with a central pore of 3nm. The structure of these forms was determined by electron microscope (EM) cryo-reconstruction to high resolution (3.2Å) [24] providing a detailed look at the structure of the infectious form of the P22 bacteriophage.

P22 is readily expressed in *E. coli* and fully assembles into the identical structure found in *Salmonella* absent of DNA. Fortunately, if only CP and SP are

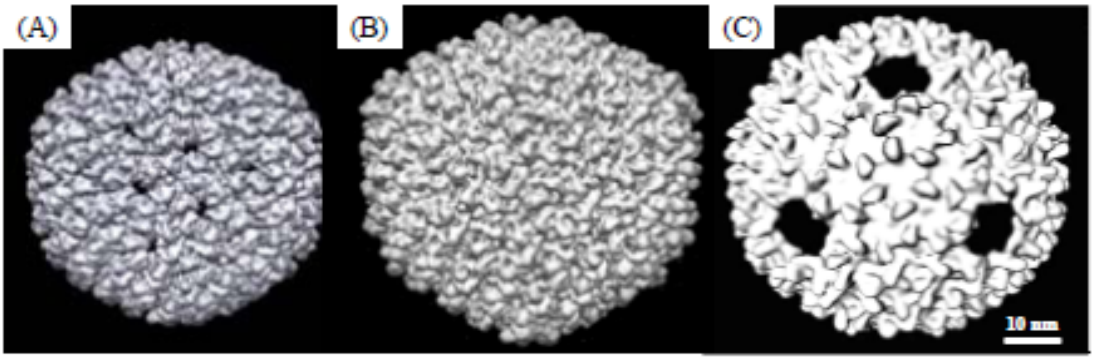


Figure 1.8: Different morphological states of P22
Space filling models showing the three different *in vitro* morphological states of the P22 . A) is the procapsid form B) is the expanded shell form C) is the wiffleball form [1].

expressed in *E. coli*, P22 assembles identically to the PC form in *Salmonella* excluding the portal complex. P22 has also been shown to assemble *in vitro* with only the CP and the SP present [88] in the same PC form (figure 1.8a). The

packaging of DNA is not the only process that causes P22 to switch conformations. DNA packaging can be mimicked thermally resulting in the release of SP and the morphological changes associated with the subunit structure making the more angular shape (figure 1.8b). By gently heating PC at 65°C for 20 minutes this *in vivo* like expansion occurs [85]. This results in a change from the spherical 58nm structure to a 64nm more angular icoshedral structure known as expanded shell (EX). SP can also be chemically extracted from the P22 capsid leaving the 58nm spherical shell fully intact, absent of SP. By treating the intact PC with 1M GuHCl the scaffold protein is removed making an empty capsid, referred to as the empty shell (ES) conformation [89]. Upon heating of the PC, ES or EX forms to 75°C for 20 minutes another form of PC is generated. All 12 pentamers are ejected from the capsid creating the form that has been dubbed “wiffleball” for its resemblance to the child’s toy [85] (figure 1.8c). This form appears to have the same 64nm outer diameter and 50nm interior diameter as EX but does not appear to have any relevance *in vivo* [85]. P22 has a number of favorable traits including but not limited to, its large size, high-resolution structure, and protease cleavage. One of the most intriguing traits of P22 is *in vivo* selection [90]. *In vivo* selection allows for the selection of capsids with desired traits such as long blood half-life, long lung residency or the ability to bind to specific tissues. *In vivo* selection is accomplished by using the well-characterized mutator strain of *salmonella*. This strain has a defective DNA polymerase that does not have the proper proofreading capabilities providing the mistakes needed to form a library of capsids. These particles are not infectious

due to the addition of the amber codon, a premature stop codon, before the tail spike gene thus preventing them from propagating on their own. Some of these proteins that incorporate mutations assemble into capsids and can be purified and assayed for mutations of interest (e.g. increased blood half-life, binding to specific substrates, etc.). After the capsids possessing the desired traits are harvested and rendered infectious by incubation with tail spike complexes, they are allowed to infect a non-mutator strain of *salmonella*. These viruses will propagate and can be purified away from the *Salmonella*. This cycle can be repeated absent of the mutator strain to ensure that there are only a small number of particles that posses the desired trait. This, combined with the many other favorable traits of P22, makes it an ideal platform for drug development, MRI imaging and other nanotechnology materials.

P22 as a Platform for Nanotechnology. The use of P22 as a material and for medical applications has only just begun with promising results. The Douglas lab developed a number of unique ways to increase the contrast with MRI agents as discussed previously and later in this work. In the past this was done in sHsp, ferritin or CCMV. Recently, a similar approach to sHsp using click chemistry has been used in P22. The maximum loading seen with sHsp was 7 Gd molecules per subunit giving a total of 168 Gd per cage. By using P22 there is evidence supporting an increase of 10 Gd ions per subunit with indication that more can be obtained giving a total of at least 4200 Gd ions per cage as is. This amount of Gd is a 25X increase of Gd ions over sHsp. By adding more Gd per cage similar

benefits to sHsp (e.g. protection of cargo and targeting) are obtained while also delivering more Gd and increasing the “brightness” of the image.

To be able to deliver something, whether a drug, an enzyme, or a protein, to a specific location while being protected from extracellular degradation could provide more effective and safer drugs. Kang et al. have shown that P22 modified to display biotin on the interior of the cage can bind streptavadin. Streptavadin has the ability to migrate through the pores in the P22 capsid, formed due to heating, and bind to the biotin [91]. Uchida et al. have shown that if the capsid is functionalized internally with phenathroline (phen) it will incorporate nickel at specific sites on the cage interior. Cytochrome C that has been functionalized with a phen group can migrate through the pores and attach to the open coordination sites on the nickel [92]. Together this demonstrates the ability to attach small proteins with different methods on the cage interior, protecting them from degradation.

Using the 10nm pores in the P22 capsid to allow for the migration of molecules has limitations regarding the molecules that can be attached (e.g. size or electrostatics). As mentioned previously truncated SP is still able to promote assembly of CP into mature capsids. Interestingly, O’Neil et al. have recently demonstrated that SP-fusion proteins, generated by addition of peptide sequences to the N-terminus of the SP, can assemble CP, resulting in a mature capsid with a non-native peptide sequence displayed on its interior. This has been demonstrated with fluorescent proteins GFP and mCherry [93]. These mutations have been sequenced and assembly confirmed by SEC, MALS, TEM

and DLS. O'Neil et al also demonstrated the ability to insert enzymes such as HIV-1-protease, superoxide dismutase and *Sso*Pox [94]. By co-assembling proteins and displaying them on the interior of the cage, enzymes can be delivered to specific cells where they can perform a necessary function that may be absent in that cell.

Other PCNs

There are other PCNs that have been mentioned in this work. However, they have not been discussed in detail. These PCNs include Cowpea chlorotic mottle virus (CCMV), human ferritin (HFn), DNA binding proteins from starved cells (Dps), and one non-protein based nano-particle a dendrimer.

Cowpea Chlorotic Mottle virus

CCMV is a member of the *Bromoviridae* family and not surprisingly it naturally infects the cowpea plant. One-hundred-eighty copies of the 20kDa coat protein assemble into a T=3 capsid with three positive sense RNA molecules

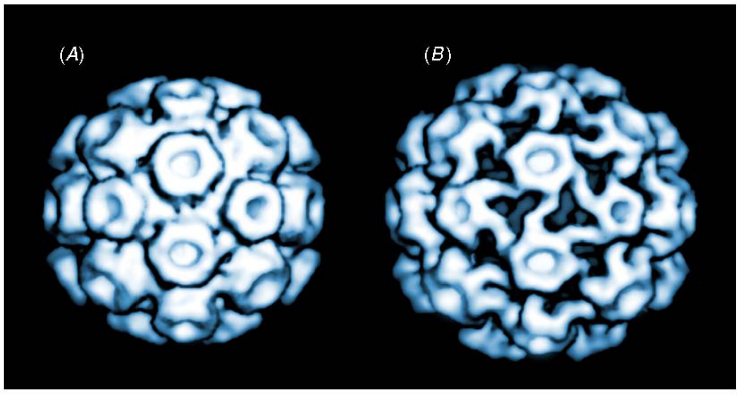


Figure 1.9: Conformations of CCMV
CCMV in its two different conformations closed (A) and open (B) [21]

packaged inside making a 28nm virus [95-97]. The crystal structure of CCMV has been solved to 2.7Å resolution revealing Ca^{2+} metal ions bound at the pseudo 3-fold axis [21, 98]. Three acidic residues (E81, E148, D153) and the carbonyl oxygen of two polar groups (Q85 and Q149) on two subunits coordinate the metal binding [21]. Interestingly, there is a reversible pH gating effect that occurs with these ions. The metal ions are released at a pH greater than 6.5 causing the capsid to swell by approximately 10% making the "open" conformation (figure 1.9b) [37]. When the pH is brought below 6.5 these metal ions will reattach making the "closed" conformation of the capsid [37] (Figure 1.9a). When in the open conformation 60, 2nm pores exist at the quasi 3-fold axis allowing for the virus to release its contents and providing bulk solvent exchange [37] (figure 1.9b). This provides the ability to trap small molecules on the interior of the cage and allows that molecule to be released in a different location [37].

CCMV has been used as an MRI contrast agent because of its natural ability to bind metals. *In vitro* the Ca^{2+} ions can be replaced with Gd^{3+} (a common MRI contrast agent). Each CCMV capsid can bind 180 Gd^{3+}ions. When Gd^{3+} is incorporated into the cage the T_1 and T_2 relaxivities were the highest reported for a molecular paramagnetic material when measured at 61 Mhz [43]. One of the main factors contributing to this high relaxivity value is the slower tumbling rate CCMV has in solution compared to a single Gd molecule. Unfortunately, the binding constant of the Gd^{3+} (31μM) was far to weak to be used for any *in vivo* applications. Gd^{3+} is an extremely toxic metal and if allowed

to exist unbound within the body it could cause severe damage if not death. In order to increase the binding constant of Gd^{3+} a metal binding motif from calmodulin (DKDGDWLEFEE) was genetically incorporated on the N terminal end of the coat protein. Gd^{3+} was incorporated into these peptides with an increase in the binding affinity [43]. However, it was still to low for *in vivo* applications.

Human Ferritin

Ferritins are found in every domain of life including bacteria, archea and eukaryotes [99-101]. They are important proteins that sequester and store iron within an organism [101]. Iron is a crucial element that gets incorporated into many proteins for both stabilizing effects and catalytic effects. However, if it remains unbound it can be toxic. Ferritins assemble into a roughly 12 nm diameter cage using 24-subunits giving them octahedral (4:3:2) symmetry [99] (figure 1.10b). Interestingly, this structure is highly conserved through all

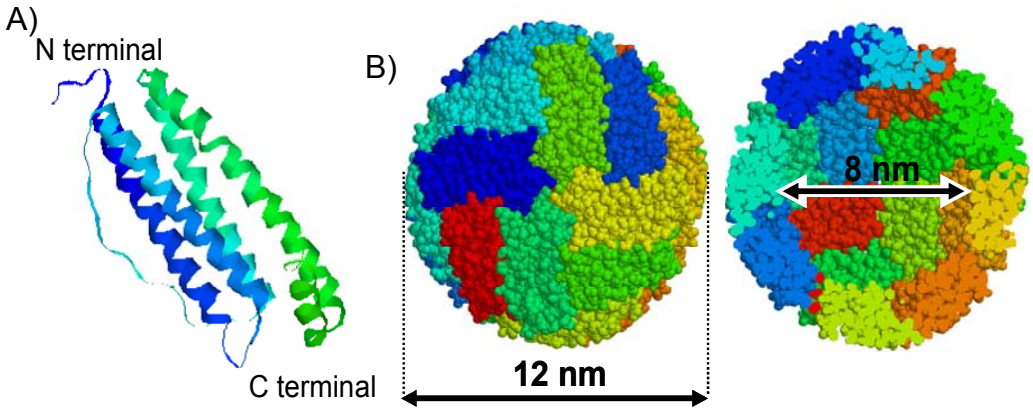


Figure 1.10: Structure of Human Ferritin
A) A ribbon diagram of the human H-chain ferritin subunit. B) space filling model of the intact ferritin cage [23].

organisms however, they vary greatly in the amino acid sequence with as little as 14% homology [99]. Ferritins contain two different chains (H and L) depending on the iron needs of the specific tissue where they are found [99]. The H-chain of the ferritin molecule contains the site that catalyzes the oxidation of two Fe^{2+} atoms and the L-chain has a role in the iron oxide core formation [99, 101]. Both the H and the L chain of the human ferritin have had their crystal structure solved to 1.52Å [23] and 1.90Å [102] respectively. With its natural ability to bind metal and form a metal oxide core there are numerous potential uses in nanotechnology.

Ferritin has been used in broad range of nanotechnology applications. The most common nano-technology use for Ferritins is as nano reaction vessels in an attempted to make nano scale metal oxide particles within the interior of the cage. Naturally the ferritin will form ferrihydrite nanoparticles. At elevated temperatures (85°C) and a pH of 8.5, magnetite (Fe_3O_4) can be formed on the cage interior. Interestingly, *in vitro* these particles are not limited to iron containing materials. Cobalt, nickel, indium, manganese and chromium oxide cores can also be formed on the interior [103-106]. Recently, ferritin with an iron oxide core has been used as a MRI dark imaging agent. A targeting peptide (RGD) that has been shown to selectively target integrins $\alpha_V \beta_3$ and $\alpha_V \beta_5$ was genetically incorporated into each of the 24 subunits displaying itself on the exterior of the cage (RGD4C-Fn). Integrin $\alpha_V \beta_3$ is known to be involved in the initiation and progression of some human diseases including rheumatoid arthritis and cancer. It has also been reported that it is found on the surface of

macrophages involved in both early and late stage atherosclerotic lesions. Uchida et al. have demonstrated the targeting of macrophages *in vitro* with this RGD4C-Fn and an iron core. As well Uchida et al. showed that when RGD4C-Fn with an iron core is injected into mice with atherosclerotic lesions, the cage targets these areas enhancing their contrast on an MRI image making them easier to diagnose. The natural ability of ferritin to form a metallic core has been harnessed and used to monitor a potentially deadly disease.

DNA Binding Protein from Starved Cells

Another PCN that has been used in materials synthesis is Dps, a member of the ferritin family [107]. Dps proteins have been found in several bacterial (*Listeria iinocua* {LiDps}) and archaeal (*Sulfolobus solfataricus* {ssDps}) organisms but have not been found in eukaryotes to date [53, 108-112]. The Dps proteins have a similar structure to ferritin but they are only comprised of 12 subunits with an exterior diameter of 9 nm [107]. To date the biological function of the Dps proteins is poorly understood however their use as constrained reaction vessels similar to that of ferritin provides a useful tool for nano-materials synthesis.

Dendrimer

Dendrimers are repeatedly branched, organic molecules that are roughly spherical in shape, monodispersed and highly symmetric. Often times the functionality of a dendrimer depends on the functional group exposed on the molecular surface [113, 114]. However, there are a few examples where

dendrimers have been internally functionalized providing the isolation of an active group similar to the active sites found in biomolecules [115, 116]. The number of repeated branching units that they contain (generations) classifies dendrimers. With each increase in generation, the molecule roughly doubles in molecular weight and provides more exposed functional groups on the exterior. Dendrimers can be made to contain any number of functional groups. These functional groups can also be altered after synthesis to customize a dendrimer for a specific function [113, 114, 117]. Poly(amidoamine) (PAMAM) dendrimers are the most well known dendrimers and are made by reacting a diamine with methyl acrylate and another diamine to form a Generation 0 dendrimer. Dendrimers have been used in nano-technology with applications ranging from drug delivery and gene therapy to nano-sensors [118-121] making them a viable source for nano-material uses.

Other PCN Not Covered in this Thesis

Many other PCNs are being explored for use in nanotechnology. Most of these PCNs are viral in origin including Cowpea mosaic virus [122], tobacco mosaic virus [123-125], the flock house virus [126], polyma virus [127], norovirus [128-130], adenovirus [131-133], bacteriophage MS2 [134], Q-beta [135], SV 40 [128-130, 136], Canine parvovirus [137, 138]. Their most common use is in biomedical applications. They have been used for materials ranging from cancer treatment to vaccines and much more. Some of the PCNs are being used to target specific cells and deliver some form of payload, while others are being

used to deliver antigens causing an immune response without the negative side effects that come with most immune responses. PCN are being used in many different areas of nanotechnology because they are easily modified and produced in high quantities. Giving them great potential to be used as drugs and materials.

Instrumentation:

Size Exclusion Chromatography

Size exclusion chromatography (SEC) is a technique that can separate molecules by size and shape. SEC is a useful technique that aids both in the purification and the analysis of proteins. There are two forms of SEC. One form uses a membrane where molecules with a specific size cannot pass through pores in the membrane. This provides a method to separate large particles from small particles. The second form of SEC uses a stationary phase made of dextran polymers, agarose, polyacylamide or silica beads and a mobile phase [139]. The resin is made of a network of neutral tunnels that vary in size. This allows the smaller particles to enter the tunnels while the larger particles are excluded. Because the smaller particles must pass though each tunnel, they take longer to flow through the resin thus eluting off the column later. Meanwhile the larger particles that did not enter the tunnels move through the resin more quickly eluting earlier [139]. Molecules are applied to the resin with a mobile phase that pushes the molecules through the resin and also aids in keeping the molecules from interacting with the resin[139]. The ideal stationary phase will

have no chemical interaction with the molecules allowing separation to be based purely on size. SEC provides an easy and simple way to separate molecules by size thus providing useful information about the molecule but also aiding in the purification of molecules.

Multi Angle Static Light Scattering

The entire molecular mass of a PCN can be extremely difficult to determine. However, light scattering has proven to be a useful tool in determining molecular mass of particles in excess of 200 MDa. Scientists such as Einstein, Raman, Debye and Zimm helped to develop the theory of light scattering and it has proven to be one of the great developments in physical chemistry. Light scattering is based on the physical property that heavier molecules scatter more light than lighter molecules (Reviewed in [140]). With this technique the average molecular weight can be determined [141, 142]. Rayleigh scattering describes the theory behind determining the molecular weight of a molecule in solution. Rayleigh scattering is the elastic scattering of light by objects considerably smaller than the wavelength. Shorter wavelengths scatter more intensely than longer wavelengths because the Rayleigh scattering is inversely proportional to the fourth power of wavelength. Scattered light detected at multiple different angles provides two critical pieces of information about a molecule. Firstly, the intensity (I_s) is proportional to the molecular weight of the particle and secondly the angular dependency of I_s is related to the radius of gyration (R_g) for the particle. The equation that defines this physical property is: $I_s(\Theta) \alpha c \times M \times$

$(dn/dc)^2$. Where I is the intensity of light scattered, c is the concentration of the scattering element, M is the molecular weight of the scattering element and dn/dc is the change in refractive index over a change in concentration of the scattering molecule. R_g is a mass distribution about the center mass. This assumes that a particle is made up of many smaller particles. Each of these particles scatters and by integrating the contribution from each of these scattering particles the R_g is determined. Since R_g is a centered mass a solid sphere will appear smaller than a hollow sphere even if they have the same hydrodynamic radius. This technique provides a simple and easy way to determine the average molecular weight of a particle in solution.

Dynamic Light Scattering

Dynamic light scattering (DLS) is a physical technique that can be used to determine the size distribution of particles in solution. As described before when light hits a particle it scatters in all directions. As this light is scattered, there is a time dependant fluctuation in the scattering intensity due to the molecules in solution undergoing Brownian motion. Due to this motion, the distance between scattering molecules is constantly changing with time. This scattered light will undergo either constructive or destructive interference by the surrounding particles. The dynamic information of a particle can be found by applying an autocorrelation function to the time dependant fluctuation. If the fluctuations are very close together the particle is moving faster and is thus smaller. If the fluctuations are father apart the particle is moving slower and is larger in

diameter. DLS is modeled on how a sphere moves in solution, therefore the hydrodynamic radius of a particle can be found. DLS is a useful technique that can provide the size of a particle.

Analytical Ultra Centrifugation

Analytical ultracentrifugation (AUC) is a technique that is used to determine molecular mass of particles in solution. This technique is valuable as it separates species based on molecular weight, size and shape. The type of AUC covered in this thesis measures the sedimentation velocity, or how fast a particle sediments from solution when spun at a high rate of speed. This sedimentation is based on the density and shape of the molecule. A sample is placed in a tube and spun at speeds upwards of 50,000 rotations per minute [139]. Using a detector the movement of the molecule is monitored as it passes through the medium thus determining when it sediments from solution. The Svedberg equation describes how molecules sediment from solution; it accounts for the rotational velocity, frictional coefficients of both the solute and the solvent, density and the molecular weight [143]. With AUC important parameters about the physical properties of a molecule can be determined. However, when PCN are modified it can be difficult to determine what effect that modification will have on how the particle sediments from solution.

CHAPTER 2

MONITORING THE STRUCTURAL TRANSITIONS IN THE BACTERIOPHAGE P22

Introduction

Tailed double stranded (ds) DNA viruses are considered to be one of the most abundant viruses on earth. Interestingly, many of these viruses share a common assembly process beginning with the precursor (procapsid) to the infectious phage. In order for these viruses to assemble properly they require a scaffold protein (SP) in addition to their coat protein (CP). They also require a portal complex that will package the DNA and also insert the DNA upon infection. This DNA packaging is accompanied by the exiting of the scaffold proteins from the procapsid and a major conformational change where the capsid swells by approximately 10% and a more angular shape is adopted.

Bacteriophage P22 is one of the most studied of these dsDNA viruses and goes through this pathway where 415 of the 46.6 kDa CP co-assemble with 60 to 300 SP subunits, 12 copies of the portal protein and 12 to 20 copies of the injection proteins making the T=7 58nm procapsid [72, 74-77]. As the DNA is packaged all of the SP subunits exit through the capsid shell and the shell expands to a 64nm icoshedral structure [72, 75-77]. When the P22 CP and SP are co-produce heterologously they will co-assemble making the 58nm procapsid structure [88]. The *in vivo* like expansions can be mimicked thermally by heating the capsid for 20 minutes at 65°C. When heated to 75°C for 20 minutes the 12

pentamers are released form the capsid making a form with no apparent biological relevance [85]. This has been dubbed “wiffleball” for its resemblance to the child’s toy.

A non-infectious viral capsid that is readily produced in large quantities in *E. coli* has the ability to be used for many different purposes such as drug delivery agents and tissue imaging. In order to use these proteins as materials a relatively easy and reproducible way to characterize these structures must exist. Here we show that the P22 capsid in its different forms can be readily characterized using multiple techniques that provide great insight into what morphological state exists. Also we show the ability to stabilize the P22 capsid to extreme temperatures with simple photo cross-linking techniques providing a high temperature platform for materials based chemistry.

Results and Discussion

Results

Binding Of OmpF To The P22 Capsid. The heterologously expressed bacteriophage P22 capsid protein (CP) and scaffold protein (SP) spontaneously co-assemble into icoshedral capsid architectures [88]. The procapsid (PC) form of P22 assembles into a spherical T=7 structure with 420 copies of the CP and a variable number of SP. P22 can assemble without the SP but adopts a range of structures including T=4 and T=7 structures [144]. When P22 CP and SP are expressed in an *E. coli* expression system multiple species are observed which

can be individually purified and characterized. In the current work, P22 was purified as previously described using ultracentrifugation and then further purified using anion exchange chromatography. Capsids elute in four distinct peaks off

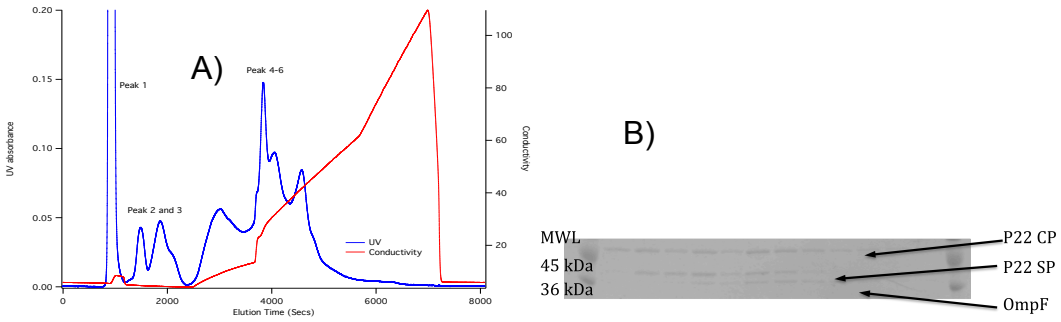


Figure 2.1: P22 purification
A) Ion exchange of P22 peak 1 is unbound P22 Peak 2 and 3 non-specifically bound protein. Peaks 4-6 are P22 with increasing amounts of OmpF protein. B) SDS-PAGE for peak tops of peak 4-6 showing increasing amount of OmpF.

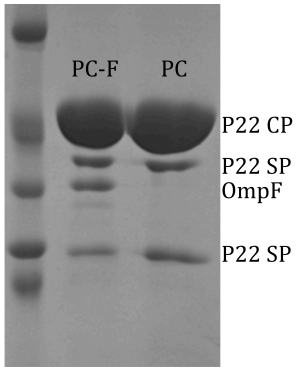


Figure 2.2: P22 SDS-PAGE
SDS PAGE gel for PC-OmpF and PC showing CP, SP and OmpF

.

the column (figure 2.1a). As determined by SDS-PAGE (Figure 2.1b) the first and broadest peak is a P22 capsid with a small number of SP (approx 98 per capsid determined by densitometry [Figure 2.2]). The second, third and fourth peaks are P22 with SP and an increasing amount of an *E. coli* protein OmpF (figure 2.1b), a host protein that appears to associate with the P22 capsid,

identified by gel digestion and mass spectrometry. We have interrogated these forms of P22 to investigate their stability and their propensity to undergo the morphological changes characteristic of the P22 capsid (PC ➔Ex; Ex ➔ WB).

In addition to SP, we have identified an additional host protein (OmpF), which is associated with the capsid in a subset of the heterologously produced P22 particles (PC-OmpF). This OmpF protein is related to the recently characterized binding of OmpA and OmpC in a related virus SF6 where these proteins are bound to the interior surface of the capsid near a quasi 3-fold axis surrounding the icoshedral 5-fold axis, between a quasi 6-fold and quasi 3-fold axis, about the icoshedral 2-fold axis, and about the icoshedral 3-fold axis. Interestingly, the binding of these proteins to the SF6 capsid is observed in both the PC and mature form of the virus (analogous to the EX form in the P22 system). It has been suggested that these proteins help stabilize the capsid as DNA is packaged much like the decorator protein of phage L or the λ phage [145, 146].

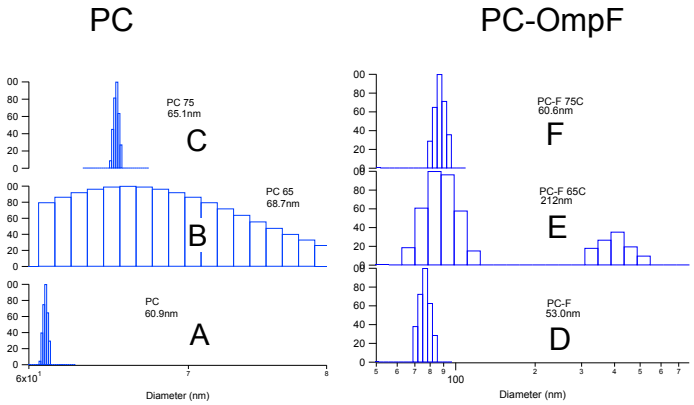


Figure 2.3: DLS of multiple forms of P22
Dynamic light scattering of PC and PC-OmpF heated to different temperatures. A,D) P22 before heating B,E) to 65°C and C,F) to 75°C

The PC and PC-OmpF forms of P22 have a spherical morphology with an expected particle radius of 27 nm, based on the near atomic resolution structures of P22. While these two forms have the same size they differ in molecular weight; PC has a theoretical molecular weight of 19.5 to 29.5 MDa (depending on the number of SP incorporated into the capsid). When measured by DLS, the R_h of the P22 PC is 25.4 nm while that of the PC-OmpF is measured as 26.5nm (Figure 2.3a,d). Using multi-angle light scattering the R_g of PC was measured as 24.3 ± 0.090nm (Figure 2.4a,d) and that of the PC-OmpF form was 26.4 ± 0.06 nm. These two complementary measurements are consistent with the expected 27nm of the P22 capsid and are consistent with TEM observation of these materials where particle diameter of 52.9±4.3nm and 53.2± 4.4nm were observed.

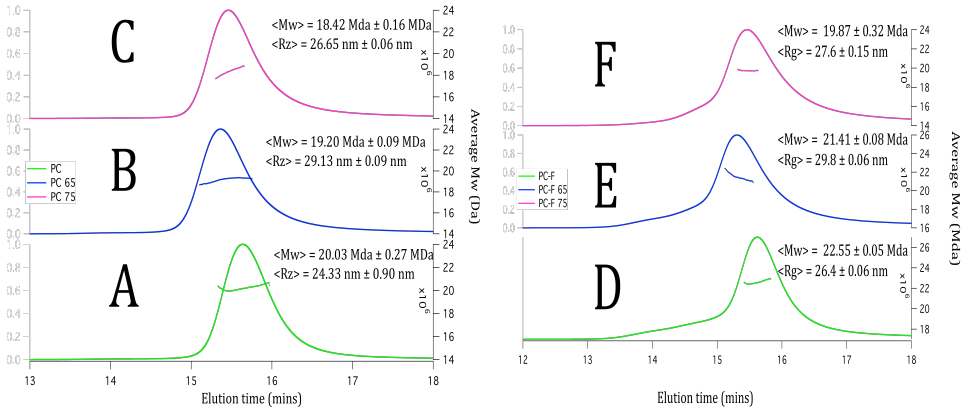


Figure 2.4: SEC-MALS multiple forms of P22
SEC-MALS of PC (A-C) and PC-OmpF (D-F) heated to different tempertaure B,E) 65°C and C,F) 75°C. The line in the center of the peak indicates how the average Mw changes across the peak.

The average molecular mass of PC and PC-OmpF forms was measured using multi-angle light scattering coupled to size exclusion chromatography

(SEC-MALS). The PC form was measured to have Mw of 20.03 ± 0.27MDa (Figure 2.4a), consistent with the T=7 capsid composed of 420 copies of the CP, each of which has molar mass of 46.6 kDa, and only 16 copies of the SP, each with a molar mass of 33.6 KDa. Using densitometry we independently estimated the ratio of CP to SP (4:1). The PC-OMPF form has Mw of 22.55 ± 0.05 MDa by MALS (Figure 2.4d) and when densitometry was performed on SDS gel showing that 79.2% of the sample is CP, 12.6% is SP and 8.2 % is OmpF. These data are consistent with a capsid having slightly less SP than the PC and approximately 70 OmpF proteins based on SDS-PAGE combined with SEC-MALS. The PC form elutes as a single peak on SEC and when the MALS data are fit across this elution profile they produce a line with a slight upward trend across the width of the peak indicating the sample is slightly polydispersed, due to differing amounts of SP within the capsid. Across the peak the Mw ranges from 19.94 MDa (14 SP) to 20.64 MDa (35 SP) (figure 2.4a). The SEC profile of the PC-OmpF form also shows a single elution peak with a similar rise in the average Mw showing that the PC-OmpF is also slightly polydispersed in the elution peak with Mw of 22.57 MDa and 22.39 MDa (figure 2.4d). This dispersity is most likely due to differing amounts of the proteins (SP and OmpF) that are encapsulated/associated with the capsid. An additional form of the procapsid, in which subunits were photo cross-linked by treatment with light, $Ru(bpy)_3^{2+}$ and ammonium persulphate (PC-X), was investigated. This material too showed R_h of 27.9nm, R_g of 27.2nm and Mw of 22.87 MDa (figure not shown), consistent with a minimally perturbed PC morphology. PC-OmpF form was also photo

cross-linked with an R_h of 27.6nm and an R_g of 30.6nm and a Mw of 23.08MDa (figure not shown).

With these materials we have investigated the changes in physical properties associated with changes in the morphology of the P22 capsid. Expansion from the PC with loss of SP and formation of a more angular 'expanded' head is associated with DNA packing in the infectious P22 virus. *In vitro*, using the heterologously expressed proteins, heating to either 65ºC or 75ºC can induce the morphological changes. Heating the PC (or ES) to 65ºC has been reported to result in the formation of an expanded form of the capsid (EX) in which the SP has been lost. Further heating, to 75ºC, has been reported to result in the formation of the wiffleball structure, where the 12 pentameric capsomeres are lost from the capsid.

Two Distinct Morphologies Are Present When P22 Is Heated To 75°C. Heating the PC form of the P22 capsid to 65ºC is accompanied by a shift in the migration on the agarose gel (figure 2.6), which can be used to detect the morphological differences in P22.

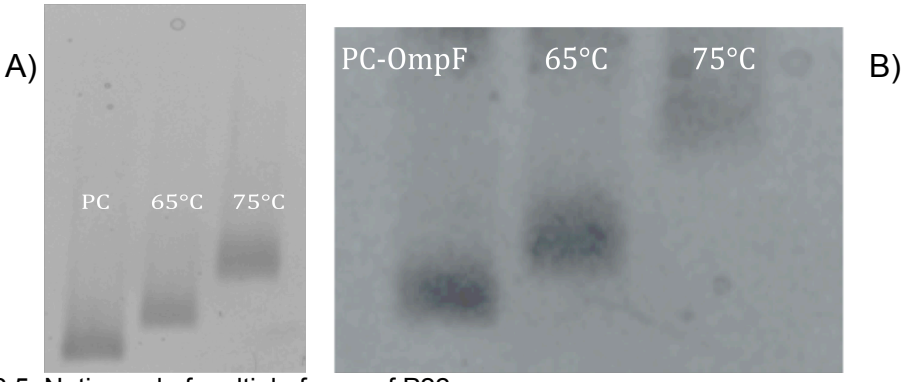


Figure 2.5: Native gel of multiple forms of P22
Agarose gel electrophoresis showing the different migration of P22 in its different morphological states.

This shift is consistent with an expected increase in diameter expected for the EX form. Analysis of the 65ºC treated material by SEC-MALS revealed that the PC sample underwent a change in size (from 24.33±0.90 to 29.13±0.09nm radius) and a significant change in mass (20.03±0.27 to 19.20±0.09MDa) (figure 2.4b) was observed. The PC-OmpF showed a similar change in size (from 26.4 to 29.8±0.06 nm radius) and was also accompanied by a change in mass (Mw 22.55±0.05 to 21.41±0.08 MDa) (figure 2.4e) consistent with loss of the encapsulated SP. Loss of the SP was additionally confirmed by SDS page of the

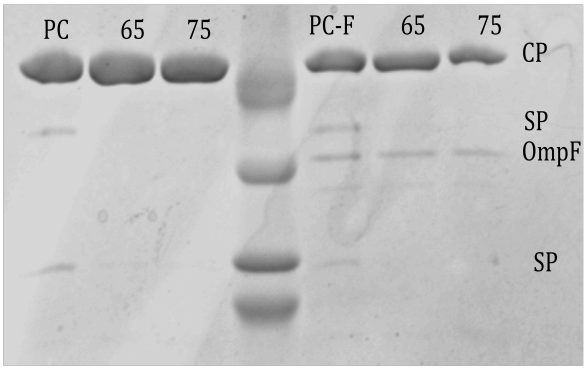


Figure 2.6: SDS-PAGE OmpF association while heating
SDS-PAGE showing that OmpF remains associated with the capsid when heated.

heated and purified sample. SDS gel of this material revealed that while the SP had been lost from the capsid, the OmpF protein remained associated with the capsid (and would account for the residual mass in this EX-OmpF form of the P22) (figure 2.6).

On heating the PC form to 75°C another shift in band position was observed by agarose gel electrophoresis (figure 2.5). SEC-MALS confirmed that

PC underwent a slight decrease in R_g (from 29.13±0.09 to 26.65±0.06nm) with a decrease in Mw (from 19.20±0.09 to 18.42±0.16MDa) (figure 2.4c). The agarose gel confirms a shift upwards in the gel. This shift has previously been reported

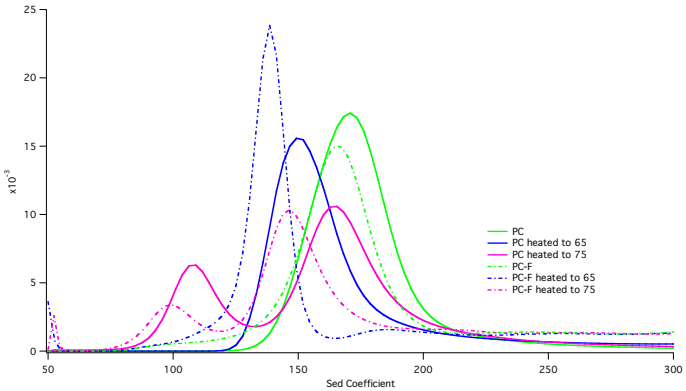


Figure 2.7: AUC of multiple forms of P22
AUC showing different sedimentation coefficients for P22 heated to different temperatures for both PC and PC-OMPF (dashed line).

as the WB form. To probe this potential distribution of species, which could not be resolved by HPLC-size exclusion chromatography or agarose gel we performed a series of analytical ultracentrifugation (AUC) analyses. The AUC

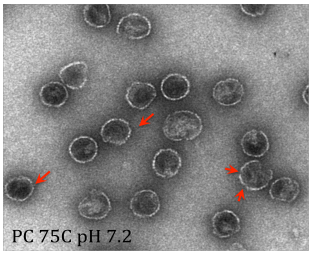


Figure 2.8: TEM of WB
TEM showing capsids with noticeable pores.

data revealed two distinct peaks, one with a sedimentation coefficient of 110 and one with a sedimentation coefficient of 170 (figure 2.7). TEM analysis confirmed the presence of structures with noticeable sections of the capsids missing,

corresponding to the missing pentamers in the WB structure (figure 2.8). A similar analysis of PC-OmpF heated to 75ºC, also showed a similar decrease in R_g (from 29.8±0.06 to 27.6±0.15nm) and a decrease in Mw (from 21.44±0.08 to 19.87±0.32MDa) (figure 2.4f). After separation via spin column SDS-PAGE confirmed that OmpF remained associated with the capsid when heated (figure 2.6). To insure that OmpF was not incorporated into vesicles and co-purified with P22 a chloroform extraction was performed on samples. Lipids were isolated from all samples. The PC-OmpF samples had a slightly higher concentration of lipids than PC but not as high as the control (P22 that has not gone through a centrifugal spin to remove large lipid aggregates) (figure 2.9). The OmpF remained in the aqueous portion and associated with the capsid (determined by SDS-PAGE) suggesting that OmpF is associated with the capsid and does not exist in vesicles. The change in Mw could be due to the loss of some, but not all,

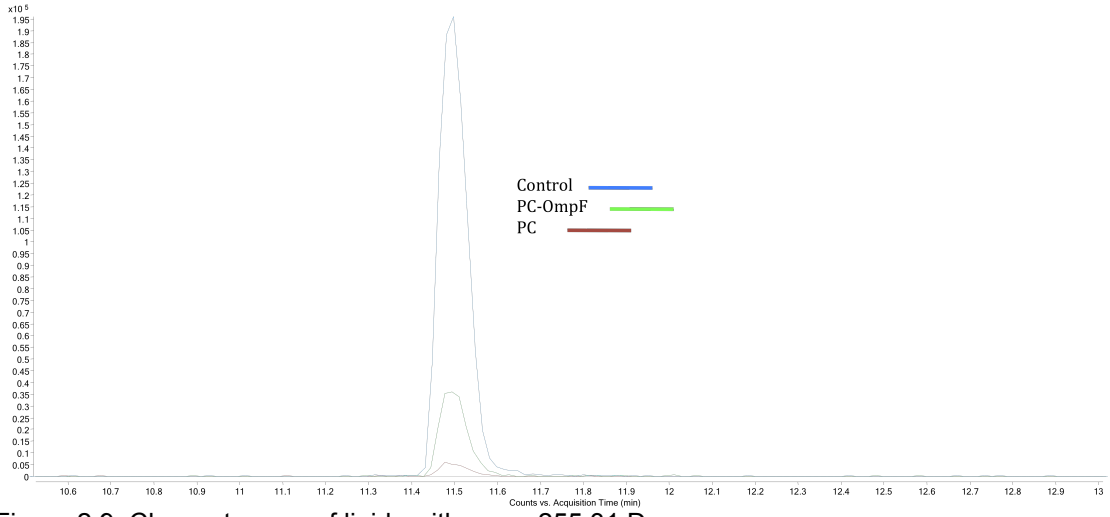


Figure 2.9: Chromatogram of lipids with mass 255.31 Da
Chromatograph showing relative amounts of lipid in purified P22. Blue) after initial sucrose gradient, green) PC-OmpF purified after ion exchange, red) PC purified after ion exchange.

of the pentamers. AUC shows that two species exist with sedimentation coefficients of 105 and 165 (figure 2.7). PC that was heated to 75°C was separated on a sucrose gradient and ultracentrifugation. Two distinct bands were seen in the gradient. These bands were separated and run SEC-MALS with an average Mw for the higher band of 14.44 MDa and an R_g of 26.8. The lower band gave an average Mw of 18.91 MDa and R_g of 27.2 (data not shown).

Photo Cross-linking Has Different Stabilizing Effect In The Presence Of OmpF. P22 PC-OmpF that has been photo cross-linked (PC-OmpF-X) becomes stabilized as compared to PC-OmpF. Monitoring the light scattering at 90° provides information about when aggregation occurs by significant increase in the amount of light scattered.

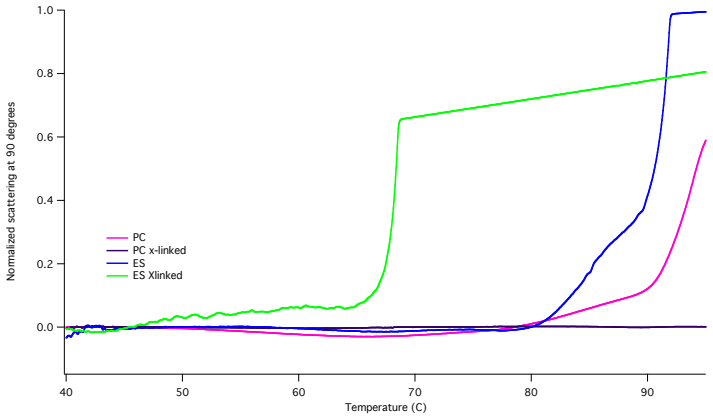


Figure 2.10: 90° SLS of cross-linked P22
90° static light scattering showing when the different forms of P22 aggregate and when the cross-linked forms aggregate.

When PC-OmpF-X is heated to 100°C it does not aggregate but remains the same size (figure 2.10). There is no significant change in the overall scattering of the PC-OmpF-X indicating that the average Mw does not change throughout

heating. PC-OmpF-X does not undergo thermal expansion monitored by the absence of a shift on agarose gel (data not shown). PC-X becomes remarkably less stable to heat. PC-X begins to aggregate at 68°C (a visible white precipitate is present when removed from the instrument) while the PC form begins aggregation at 82°C (figure 2.10). DLS and SEC-MALS also confirm that there is no change in the diameter or the Mw when PC-OmpF-X is heated to 100°C (data not shown).

pH Stability. We have also investigated the stability of P22 capsid over the pH range of 4 to 8 to see what affect pH has on the morphological transitions of the capsid. PC remained stable at room temperature in all pH values tested (4,5,6,7.2 and 7.9) based on agarose gel (Figure 2.11) and DLS. When heated (to 65ºC) at pH 4 most of the capsid aggregated and precipitated from solution based on visible white pellet when centrifuged and little to no DLS reading. TEM shows that some capsids did remain in solution and transformed to the more

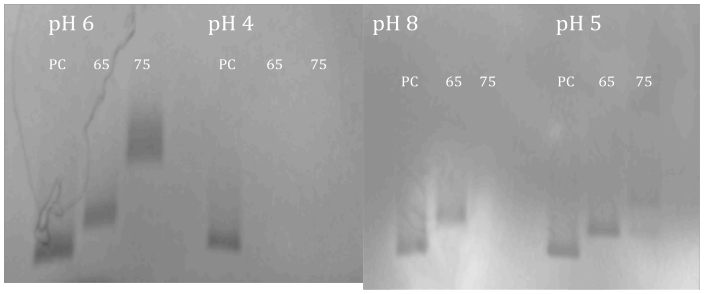


Figure 2.11: Transitions in P22 at different pH
Agarose gel showing the transformations of P22 at different pH.

angular shape (EX). No intact capsids could be found when heated to 75°C at pH 4. SEC-MALS could not be performed on pH 4 samples as the material irreversibly absorbed to the SEC column. Samples at pH 5 also showed the

unique shifts that have been associated with the morphological changes of P22 by agarose gel (figure 2.11). Interestingly, when heated to 75°C there are 4 distinct bands. One of the bands corresponds to EX that was not transformed to WB. The other two bands appear much higher on the gel indicating larger particles (figure 2.11). DLS shows that the diameter is slight higher than expected before heating (72nm). However, when heated the diameter drops to the expected values for both EX (65nm) and WB (63nm). DLS also shows the appearance of larger diameter (≈200nm) particles when heated to both 65C and 75C. The P22 at pH 5 also interacted with the SEC column preventing Mw measurements. Samples heated at pH 6 were analyzed by agarose gel which indicated the formation of EX at 65ºC and WB structure after heating to 75ºC (figure 2.11). TEM of these samples revealed capsids with the angular shape when heated to 65°C and some capsids appeared to have pores when heated to 75°C, confirming the morphological transitions. Average Mw for the pH 6 samples was determined by SEC-MALS. PC had an average Mw of 19.88±0.35MDa. When heated to 65°C the average weight dropped slightly as expected to 19.79±0.15MDa. When heated to 75°C the Mw dropped slightly more than expected (17.99±0.25MDa) (Figure 2.12a) indicating that perhaps slightly more sample converted to WB. Samples treated at pH 7.9 show a similar behavior to samples at pH 7.2, but there was a measurable difference in the capsid diameter 23.5nm vs. 24.33nm for PC and 27.1nm vs. 29.13nm for EX. The average Mw remained about the same at 19.94MDa for PC 18.84MDa for

the 65ºC heated sample (EX) and 18.43MDa for the sample heated to 75ºC (WB) (Figure 2.12b and c).

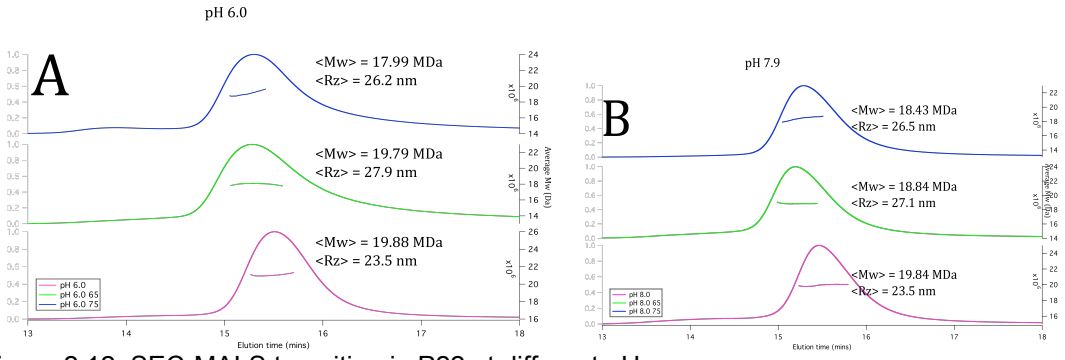


Figure 2.12: SEC-MALS transition in P22 at different pH
SEC-MALS showing the transitions as P22 is heated to different temepratures and the average Mw of those transitions at different pH values A) pH 6 B) pH 7.9.

Discussion

Two Distinct Morphologies Are Present When P22 Is Heated To 75°C. Our results clearly indicate that when P22 is heated to 65°C *in vitro* it transforms to an expanded form of the capsid and the morphology mimics the *in vivo* expansion caused by DNA packaging. In addition, we report that when heated to 75°C two distinct morphologies are present. Previous studies have shown the existence of one form termed WB where the pentons have been released from the capsid resulting in the formation of large 10 nm pores through the capsid shell. Samples of the P22 procapsid that were heated to 75°C show two distinct species by AUC, although they could not be resolved by size exclusion chromatography. When these peaks are separated by sucrose gradient and imaged with negative-

stain electron microscopy the morphologies are clearly different (figure 2.13). One morphology contains large pores on the exterior of the capsid (figure 2.13a and b) and one does not contain any apparent pores (figure 2.13c). This

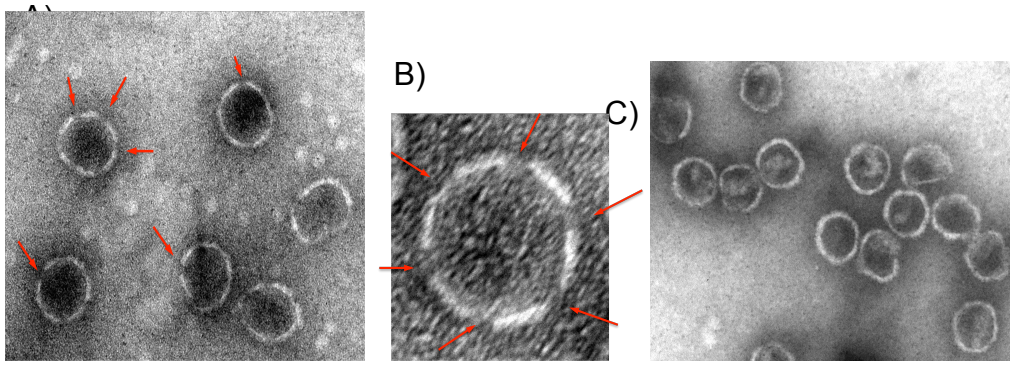


Figure 2.13: TEM of different morphologies
TEM images showing the different morphologies that were seperated out by sucrose gradient. A&B) WB C) modified EX

structure without pores does not appear to have the angular shape that is commonly seen when samples are expanded at 65°C. This species is clearly not consistent with the EX morphology. This species is smaller in radius and appears slightly heavier than EX by AUC and migrates to the same distance as P22 PC that has been heated to 75°C on agarose gel (figure 2.14). If P22

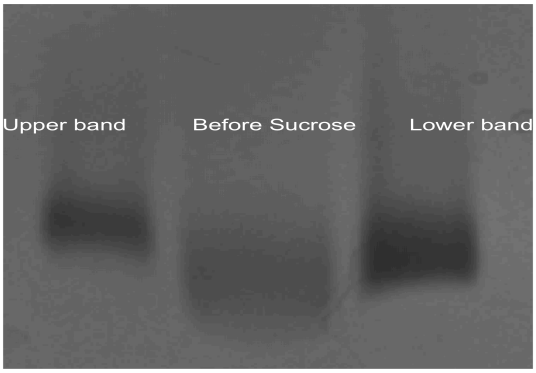


Figure 2.14: Native gel of P22 heated to 75
Agarose gel showing how the migration of the different bands from sucrose gradient.

remains at 75°C for longer periods of time (1 hr) the same distribution of WB is seen. Thus, we suggest that this is a T=7 capsid that has undergone a slight structural change becoming slightly smaller but does not lose its pentamers.

Binding Of OmpF To The P22 Capsid. We have identified two different PC species in P22 samples heterologously expressed. One of these species is P22 assembled with SP the other incorporates an additional *E. coli* protein (OmpF) apparently attached to the outside of the capsid. A homologous protein exists in P22 host *Salmonella typhimurium* and we were able to show that this protein too will bind to the P22 capsid simply by incubation with *Salmonella* cell lysate (figure 2.15). Many dsDNA bacteriophages show the ability to stabilize their expanded structures by binding other proteins or covalent modifications to

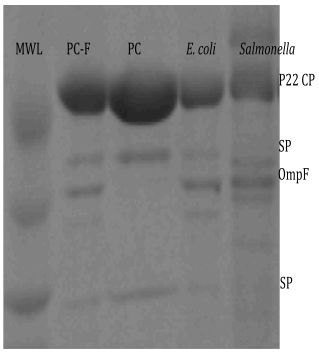


Figure 2.15: SDS-PAGE binding of OmpF
PC was added to cell lysate to confirm binding after capsid assembly.

their capsid proteins. This is most likely to protect the capsid from exploding under the enormous pressures (60 atm) that are applied to the capsids when DNA is packaged. HK97 shows a covalent cross-linking that occurs naturally between subunits [147], while phage L and the λ phage shows the use of another protein, decorator (dec) and gpD [146, 148] respectively, that will only attach to

the expanded form of the capsid. These proteins has been shown to stabilize the capsid during DNA packaging. Recently, other outer membrane proteins were shown to be incorporated within the Sf6 bacteriophage and it has been suggested that they may have a stabilizing effect. It is strange to believe that an outer membrane protein has the ability to be incorporated into a viral capsid prior to exit from the cell. However, it has recently been suggested that during viral infection the osmotic stress on a cell is significant and leads to the up-regulation of many outer membrane pores that help to relieve osmotic stress. OmpF is an outer membrane pore that transports ions to control osmotic pressure. Cells may be undergoing similar osmotic stress when heterologously expressing proteins in large quantities thus causing the up-regulation of these outer membrane pores allowing for their incorporation/association with the P22 capsid. OmpF has the ability to bind to the P22 capsid both *in vivo* and when heterologously expressed. The binding of the OmpF protein does not appear to effect the morphological transitions in P22. P22 still has the ability to form the EX and the WB structures. However the binding of the OmpF does appear to slightly stabilize the capsid at extreme temperatures causing the protein to aggregate at slightly higher temperatures than PC alone (figure 2.10). OmpF may be a stabilizing protein that associates with the P22 capsid during assembly in order to help stabilize the structure when placed under extreme stress (DNA packaging).

pH Stability. To our knowledge, the *in vitro* pH stability of the P22 capsid has not been thoroughly explored. We have shown that the PC form of P22 is

stable at a pH range of 4 to 8. PC transforms into its different morphological states between pH 5 and 8, when heated, but at pH 4 and below the PC is not stable to temperatures of 65°C or above and the capsid tends to aggregate. This suggests a window of conditions in which the P22 capsid might be useful as a synthetic material.

Photo Cross-linking Has Different Stabilizing Effect In The Presence Of OmpF. Aggregation of the P22 capsid occurs between 80 and 90°C however, photo cross-linking in samples that contained bound OmpF protein appeared to stabilize the P22 architecture. Photo cross-linking usually involves tyrosine cross-linking and the majority of the tyrosine in the assembled capsid are located at the subunit interface within the hexamers and pentamers. There does not appear to be any tyrosine poised to cross-link across the hexamer:pentamer interface. PC-OmpF-X is stable to 100°C with little to no change in average Mw or particle size. The OmpF protein is tyrosine rich and might crosslink to the P22 capsid acting as a staple to stabilize the structure and prevent the normal thermal transitions (to EX and WB) that are typically seen in P22. The cross-linking of the OmpF to the capsid has the ability to lock the capsid in the PC morphology. The photo cross-linking of PC-OmpF-X provides an ultra stable platform for future modifications to the capsid.

Conclusion

The *in vivo* assembly and morphology of P22 has been very well characterized. However, there is little known about the conformation of recombinant P22. Presented here is data demonstrating that heterologously expressed P22 exists in multiple, previously not described, morphologies. Notably, two forms of the P22 procapsid have been isolated. One consisting of the P22 CP and SP assembled into a 58nm structure similar to that found *in vivo* without the portal complex. The second form also comprises P22 CP and SP assembled into the same 58nm structure but it also contains OmpF. While OmpF does not appear to effect the *in vitro* morphological transitions of P22 it does somewhat stabilize the capsid from aggregation compared to P22 without OmpF. Another form of P22 has also been isolated and described here. When P22 is heated to 75°C two forms are observed in solution. One form is similar in structure to the previously described “wiffleball” while the other form has not been previously described. This form has a spherical morphology with an approximately 60nm diameter containing all 420 CP, smaller than what is expected for the expanded shell form and larger than expected for the procapsid form a compressed EX form.

In order to use P22 for materials synthesis a more thorough understanding of its stability under various chemical and environmental conditions must be obtained. Here it is demonstrated that P22 remains stable in solution from pH 4 to 8. While the capsid is stable in these conditions it does not go thorough the

above-mentioned morphological transitions at pH 4. As it is heated at pH 4 the capsid aggregates from solution showing that it is stable at low temperatures but not at elevated temperatures. P22 in a pH range of 5 to 8 remains stable and exhibits all morphological transitions.

An ultra-stable P22 platform would be ideal for materials synthesis as it would likely remain intact under the range of chemical and environmental conditions necessary for diverse types of modifications. The data presented above demonstrate that by photo cross-linking the P22-OmpF capsid an ultra stable platform can be formed, with stability of the intact quaternary structure up to 100°C. Surprisingly, when the capsid absent of OmpF is photo cross-linked it becomes remarkably less stable and aggregates from solution at 65°C. Interestingly, this is where P22 begins its morphological transition suggesting that this cross-linking alters the capsids ability to undergo these morphological transitions. The P22 platform shows a diverse range of applications including nanomaterials synthesis and biomedical applications. This work is critical for understanding how the capsid will respond in conditions that are likely to be present in various syntheses.

CHAPTER 3

UNDERSTANDING THE MECHANISM FOR THE PRODUCTION OF INDUCED BRONCHIAL ASSOCIATED LYMPHOID TISSUE WITH PROTEIN CAGE NANOPARTICLES

iBALT- Structure And Function

The human immune system is a complex network of biomolecules, cells and organs that function to protect the body from infection and disease. There are two “arms” of the human immune system[149]. One arm is the innate immune system and is the frontline of defense designed to quickly protect the body from common infections caused by bacteria and viruses. The innate immune response is notable for its rapid initiation and generally targets non-specific antigens such as common lipopolysaccharides displayed on the surface of bacterial cells[150]. The other arm provides the main effector mechanisms for clearance of infection and prolonged immunity and is known as the adaptive component. An adaptive immune response takes longer than the innate response to initiate but is highly specific for its target[150]. After the adaptive immune response has rid the body from infection, prolonged immunity is maintained through the establishment of memory T and B cells. These persist in specialized tissues for an extended amount of time. The memory cells can then be quickly activated to prime a secondary response following a subsequent infection of the same or similar pathogen[150]. The primary adaptive immune response is initiated in the secondary lymphoid organs such as lymph nodes, Peyer’s patches or the spleen[149]. These organs recruit naïve lymphocytes

from the blood and promote their interaction with the antigen-presenting cells[149]. After the lymphocytes are activated and replicated, they move to the infected areas to perform the effector function[149].

The primary and secondary lymphoid organs are critical to forming an adaptive immune response[151, 152]. Not surprisingly, mice that are lacking these organs are unable to mount a primary immune response to pathogens, antigens and allografts[153-155]. However, it has been shown that if these mice that are exposed to some respiratory pathogens, including influenza and *Pneumocystis*, they are still capable of producing antigen specific B and T cells[156, 157]. It has been hypothesized that bone marrow may function as a lymphocyte priming tissue for systemic infections in the absence of other lymphoid tissues. However, an emerging paradigm is that bronchial associated

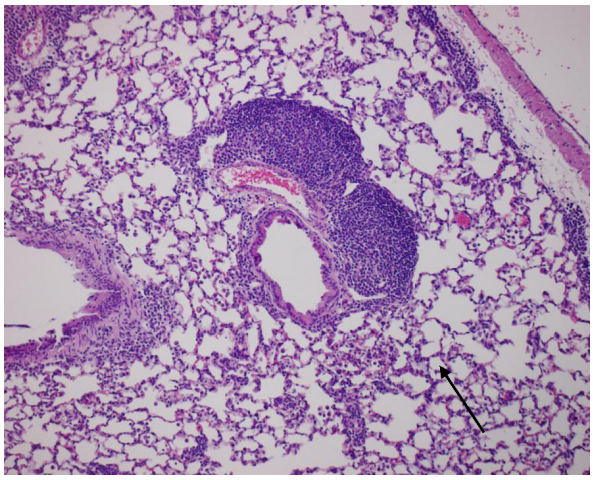


Figure 3.1: iBALT structure
Histology showing iBALT formed in the lung of a mouse that was given sHsp.

lymphoid tissue (BALT) may be responsible for initiating a primary and secondary immune response in some cases. The formation of these tertiary lymphoid tissues is typically associated with chronic infection and inflammation[156]. However, tertiary lymphoid tissues are similar in structure to the secondary lymphoid tissues in which T and B cells organize into distinct regions and are in close proximity with dendritic cells[158]. They are distinct because they are not connected to afferent lymphatic vessels and they are transient in nature. In order for the tertiary lymphoid tissue to remain, there must be a continual presence of antigen[156]. These tissues are referred to as induced BALT (iBALT) (figure 3.1) because they are formed in the presence of an infection and not stochastically.

iBALT is formed in the lung in response to prolonged stimulation by some antigens. They form in the interstitial spaces of the lung and are closely associated with the blood vessels[156, 159]. These tissues are in close proximity to mucosal surfaces, which may aid in the rapid acquisition of pathogens and antigens from the airways[160]. Although the manner of acquisition of antigens in iBALT is poorly understood, it may be through an M-cell-like mechanism. The co-localization of dendritic cells also indicates that the antigen presenting cells may be involved in the delivery of the antigen to the lymphocytes[160]. iBALT have been shown to protect against select viral infections in mice that lack secondary lymphoid tissues although with delayed kinetics. The delayed kinetics showed lower initial numbers of influenza specific CD8 T cells and low antibody titers. However, 14 days post infection these influenza specific CD8 T cells and the antibody titers were similar to those in the

wild type controls[155]. Surprisingly, the mice that relied solely on iBALT for protection had significantly reduced mortality even when infected with higher viral doses than the wild type controls[155]. This may be due to the fact that iBALT-induced responses do not exhibit the pulmonary inflammation typically associated with conventional influenza responses.

The delay in the kinetics associated with an iBALT immune response is most likely due to the need to form these tissues after exposure to an antigen. It has been proposed that this is why iBALT mediated responses are typically overlooked. This is due to the relatively rapid establishment of the conventional secondary lymphoid immune response. However, pre-established iBALT tissues in the lung are able to quickly generate a primary immune response[67]. Wiley et al. have shown that the clearance of influenza infection was accelerated if this infection is established during the immune response of a previous infection to *Pneumocystys murinia*, an unrelated pathogen[67]. Titers of anti-influenza antibodies were increased in mice that had been treated with *Pneumocystis* and displayed decreased morbidity to the control group. Recently, Wiley et al. have shown that intranasal pretreatment with the PCN sHsp produced iBALT structures[66]. This pretreatment has similar protective ability as the pretreatment of *Pneumocystis*. Also, pretreatment with the PCN shows protection to other respiratory viruses such as SARS-CoV (a mouse model) and RSV-like paramyxovirus[66].

The lung is not typically targeted in drug delivery because of its high susceptibility to inflammation damage. This can lead to drastic consequences

when delivering a drug and attempting to induce an immune response. However, the introduction of the sHsp cage into the lungs does not appear to have any negative consequences, and may actually attenuate pulmonary inflammation[66]. Ovalbumin-sensitized mice were given the sHsp cage and then challenged ovalbumin which have a strong response when given methacholine and monitored for airway hypersensitivity, testing the susceptibility to asthma (a good indication of the damage in the lung). Those mice that received sHsp showed significantly less breathing difficulty than those that were treated with buffer alone[66]. Interestingly, the mice that were pre-treated with sHsp also had less trouble breathing than those that were not ovalbumin-sensitized. Mice that are given sHsp not only significantly accelerates respiratory virus clearance after primary infection but also results in a host immune response that causes less lung damage[66].

Currently vaccine strategies are often hindered due to a lack of information regarding suitable antigens. This is further complicated in the case of rapidly mutating viruses such as influenza. It is hypothesized that PCN-induced iBALT may provide a prophylaxis against some respiratory viruses. This may facilitate aid workers entering an area with a pandemic without the need of vaccination, or may improve protection while new vaccines are being developed. sHsp has additional potential as a bona fide vaccine in that attachment of specific antigens is feasible. This would allow for the iBALT to be formed and antigens presented to these cells causing an immune response in which antibodies could be formed to those antigens protecting the person.

The mechanism for iBALT production is poorly understood. However, to date the only agents associated with iBALT production have a particulate nature including a small suite of viral, fungal and some bacterial pathogens as well as some PCN[66, 67, 151, 161]. It is unknown what features of PCN are responsible for induction of iBALT, however, it has been observed that not all PCN are equally effective. For example, (HFn), despite being similar to sHsp in size and quaternary structure, does not induce iBALT as significantly as sHsp (figure 3.2).

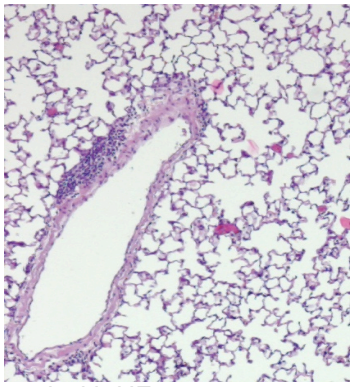
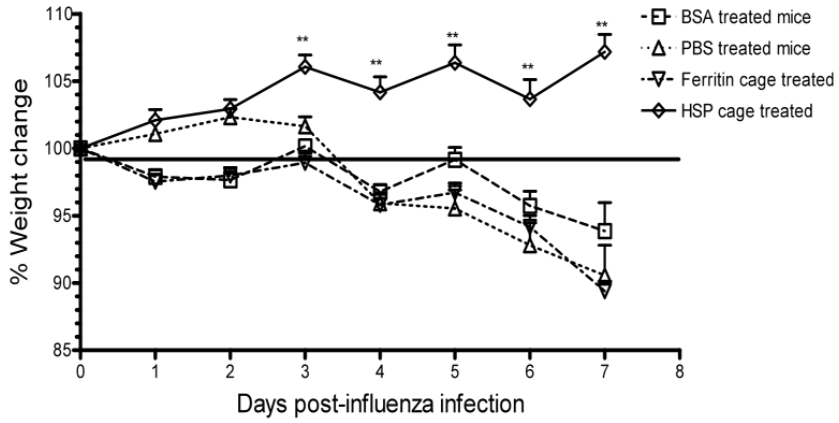


Figure 3.2: Histology from mice treated with HFn
Histology showing small iBALT formation in Hfn treated mouse.



**, P<0.01 - HSP treated group relative to each of the other groups.

Figure 3.3: Mice treated with different proteins
Naïve mice were pretreated with PCN (sHsp or ferritin) and subsequently challenged with influenza. Morbidity in ferritin treated mice was indistinguishable form control mice.

Although, HFn decreases the viral burden of an influenza infection it is still 100 fold greater than the viral burden for those mice pre-treated with sHsp. HFN also provides some amount of protection as determined by weight lose (figure 3.3) but it is significantly less protection that that observed with the sHsp, suggesting that it is not a generic feature of all PCN. Although mice were treated with a fully intact quaternary structure of the sHsp it is unclear how sHsp exists *in vivo*. It was previously shown that the intact sHsp cage exists in a dynamic equilibrium with its subunits; a feature not seen in the HFn cage. Interestingly, an externally cross-linked sHsp, which does not undergo subunit exchange, does not exhibit the same iBALT production that is observed in native sHsp. It is possible that subunit exchange, or some sort of dynamic structural plasticity, plays a role in PCN-mediated iBALT responses.

Destabilizing The sHsp Cage

Structural plasticity may play a role in iBALT formation. It has been shown that HFn, which does not produce iBALT as well as sHsp, does not undergo subunit exchange. As well an externally cross-linked sHsp does not produce robust iBALT. Due to this preliminary research it is hypothesized that because of the dynamic nature of the sHsp it is easier for antigen presenting cells to process the cage and develop an immune response. Structural plasticity is not the only mechanism that may lead to iBALT formation. There are numerous other mechanisms that can induce on immune response that mat lead to iBALT formation. There may be a small primary or secondary structure within the PCN

that triggers an immune response leading to the formation of iBALT. The sHsp has been shown to interact at the interstitial spaces within the lung. It has been hypothesized that the sHsp may be aggregating together in these areas, which may have induce this robust iBALT response. However, there is very little known about the mechanism that causes this robust iBALT response.

To determine if this dynamic equilibrium has an effect on iBALT production, we generated a destabilized sHsp construct. From the atomic resolution structure, key interactions at the subunit interface were determined. These interactions included five sets of potential salt bridges including E92:K55, R93:D51, E98K:R107, K141:E78 and K142:E117 (figure 3.4). In order to destabilize these salt bridges, mutations were generated using standard PCR

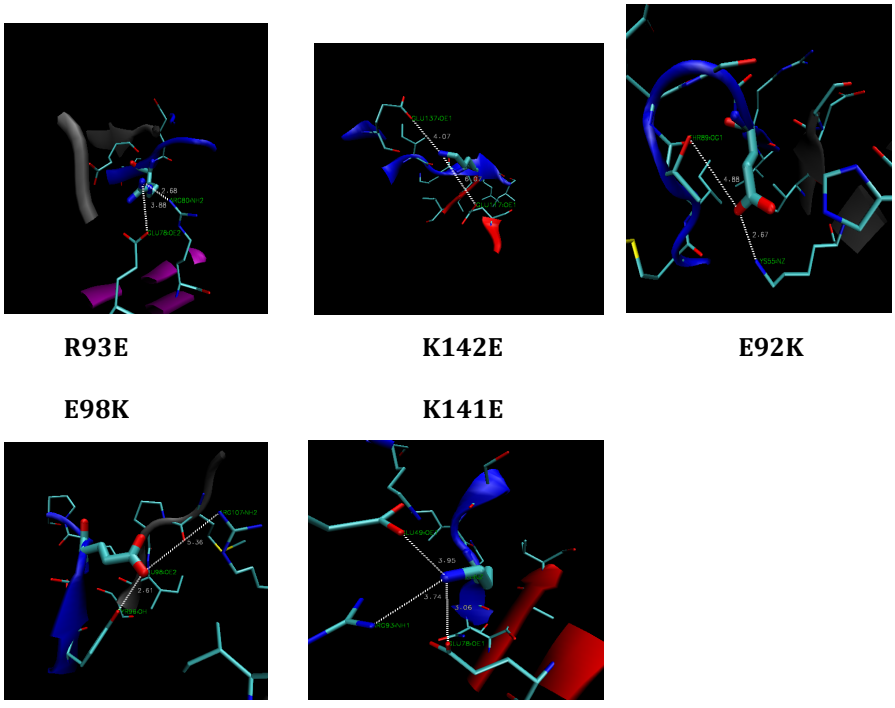


Figure 3.4: Destabilizing mutations made in sHsp
Projections showing amino acids to that were altered and their potential binding partners. Distances to there nearest neighbors are in white within the figure. Made using VMD.

methodologies. The mutations that were generated were R93E and K142E determined by DNA sequencing. Purification was performed in the same manner as native sHsp. SDS-PAGE gel and mass spectrometry also confirm the correc

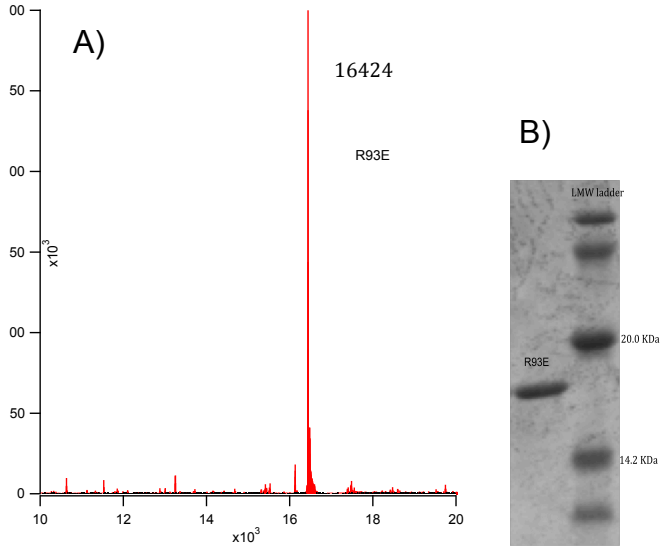


Figure 3.5: R93E Subunit mass
A) Mass spectrometry showing correct subunit mass for sHsp R93E B) SDS-PAGE gel showing correct migration for sHsp R93E.

subunit mass while MALS confirms the correct mass of the cage (figure 3.5). R93E purified as expected and assembles into an intact 12nm cage shown by DLS and SEC (figure 3.6). K142E did not purify in the same manner as native

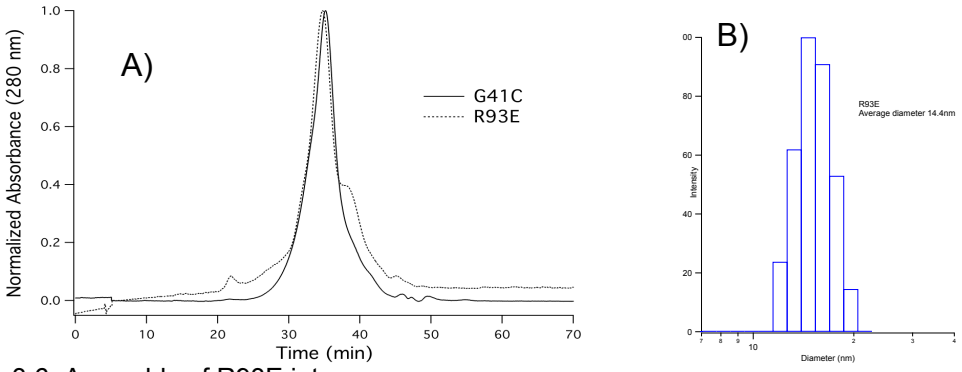


Figure 3.6: Assembly of R93E into a cage
A) SEC and B) DLS showing that R93E assembles into an intact cage with a similar diameter to native sHsp.

sHsp. K142E appeared to be isolated in exclusion bodies as it was seen in the cell pellet after lysis. In an attempt to purify K142E from these exclusion bodies a protocol that requires the denaturing of the protein was attempted. Although, K142E was isolated using this protocol (confirmed by mass spectrometry) no method was found that allowed for the refolding of the K142E mutation (data not shown). In an attempt to determine if there was altered stability in the sHsp mutation, heat stability was monitored. This would give an initial indication if the cage had been successfully destabilized. Although, it has previously been reported that sHsp is stable above 90°C, 90° SLS shows that while stable to 100°C the cage appears to disassemble into smaller subunits (figure 3.7). This disassembly is completely reversible and cage will reassemble into the 12nm structure when brought back to room temperature (figure 3.7). This

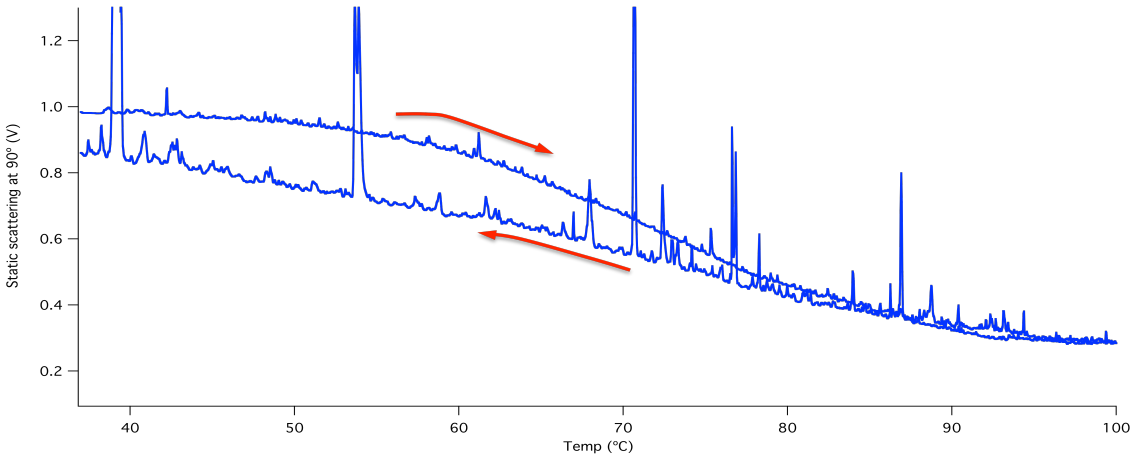


Figure 3.7: 90° static scattering of G41C
90° static light scattering monitored while G41C is heated from 37°C to 100°C and back to 37°C.

disassembly/reassembly does not appear to happen in the R93E mutation as SLS shows that R93E aggregates from solution at 98°C suggesting a difference

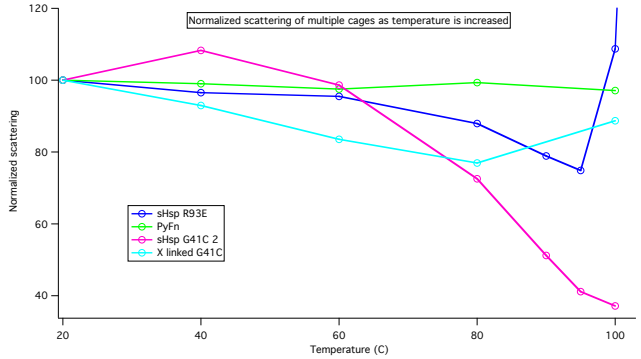


Figure 3.8: 90° SLS of multiple PCN
90° SLS of multiple PCN showing the disassembly and stability of G41C, R93E, cross-linked sHsp and PyFn as it is heated to 100°C.

in the stability of the cage (figure 3.8). For comparison SLS was performed on an internally cross-linked sHsp, which shows a slight decrease in scattering intensity, although not as much as observed with G41C sHsp (figure 3.8). This decrease may be due to a small population of sHsp cages with incomplete cross-linking. This disassembly/reassembly does not have an effect on the secondary structure of the protein confirmed by CD spectroscopy (figure 3.9).

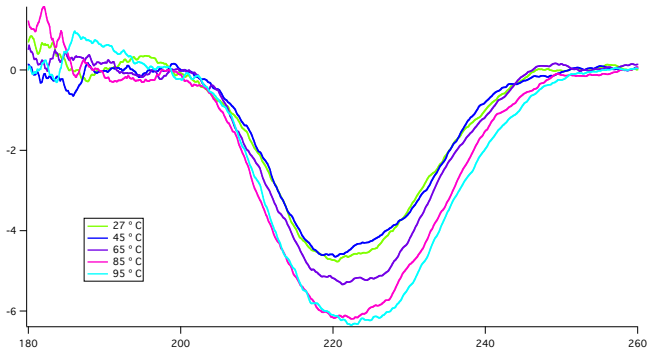


Figure 3.9: CD of G41C
CD spectroscopy of G41C while heated.

The data presented above suggest that there is a slight destabilizing effect in the R93E mutation. It also appears that it does not disassemble in the same manner as the G41C mutation.

Induction Of iBALT With Different PCN

In order to probe the effect of PCN stability on iBALT responses a suite of PCN was monitored for the capacity to generate iBALT. These PCNs include P22, a DNA binding protein from starved cells (DPS), CCMV, HFn, an internally cross-linked sHsp and a generation 4.5 dendrimer (although not a PCN but an organic particle with the same diameter as sHsp) (figure 3.10). These PCNs were selected because each has a high-resolution structure and the ability to be chemically and/or genetically modified.

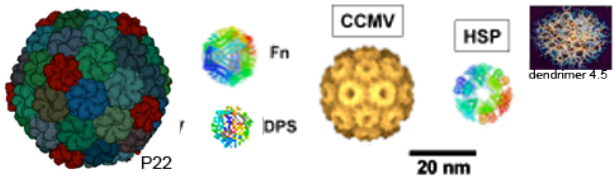


Figure 3.10: PCN used in mice
Space filling images of protein PCNs given to mice.

Mice were given five doses of 100μg of protein in solution (PBS pH 7.2) intranasally to six mice per cage. While the same weight of PCN is being delivered because the PCN varies greatly in mass considerably fewer particles are being delivered in PCN that weigh more (Table 2.1). The PCN needs to be processed so fewer particles are being delivered. This means that not as many antigen-presenting cells are going to come in contact with the PCN, which may

Table 2.1: number of particles delivered

PCN	sHsp	P22	CCMV	DPS	x-linked sHsp	dendrimer	Control
# of particles	$1.51x10^{14}$	$3.09x10^{12}$	$1.65x10^{13}$	$1.39x10^{14}$	$1.51x10^{14}$	$2.29x10^{15}$	0

The number of particles being delivered to each mouse per dose of PCN.

affect the frequency of iBALT formation. These five doses were delivered over a two-week period to allow iBALT enough time to form in the lungs, thus producing the strongest response possible. After the fifth dose, the mice were allowed three days before inoculation with influenza. A mouse for each PCN was sacrificed and tissues prepared for histology. Mice were then inoculated with a 1500 plaque forming units (PFU) solution of the mouse adapted influenza strain PR8. Mice were weighed every day to monitor their health and body weight.

Body weight is a good indication of how well mice are handling an infection as loss of body weight suggests the mice are becoming ill. Mice were sacrificed seven days post infection at which point blood was taken to look for influenza specific IgG. Broncho-aveolar lavage fluid (BALF) was collected to look for lung associated IgG and IgA antibodies. The lungs were harvested from the mice to determine viral burden in the lungs indicating how resolved the infection was.

The formation of iBALT structures in the lungs of mice treated with both the sHsp and the bacteriophage P22 (figure 3.13) along with significantly lower amount of weight loss in these mice is indicative that protection against some respiratory viruses can be obtained with multiple PCN (figure 3.11). However,

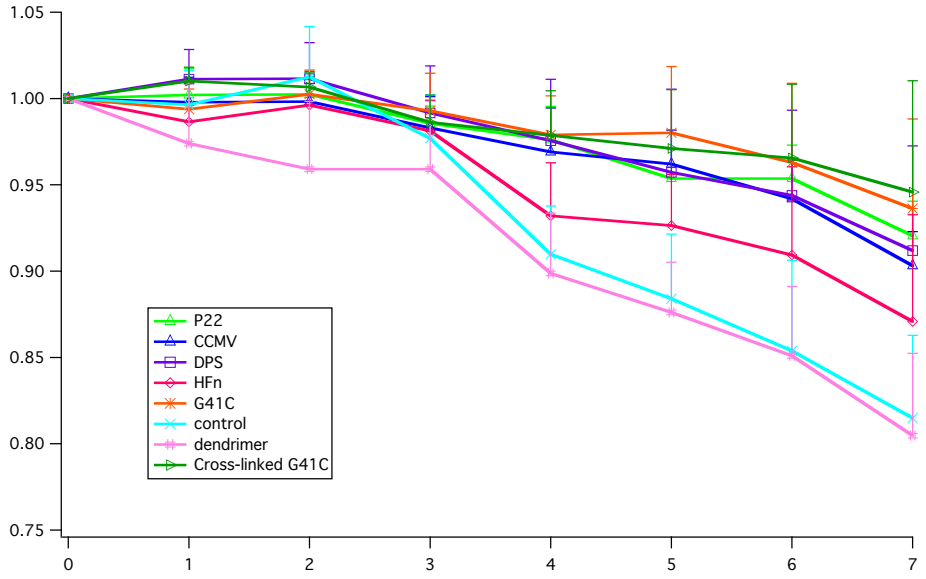


Figure 3.11: Percent weight lose for mice given multiple PCN
Naïve mice were treated with different PCN. Body weight was monitored for seven days. sHsp (native and cross-linked) were better than other PCNs while P22 still provide good protection. Other PCN also provided protection while the dendrimer and Hfn were significantly worse than the other PCN.

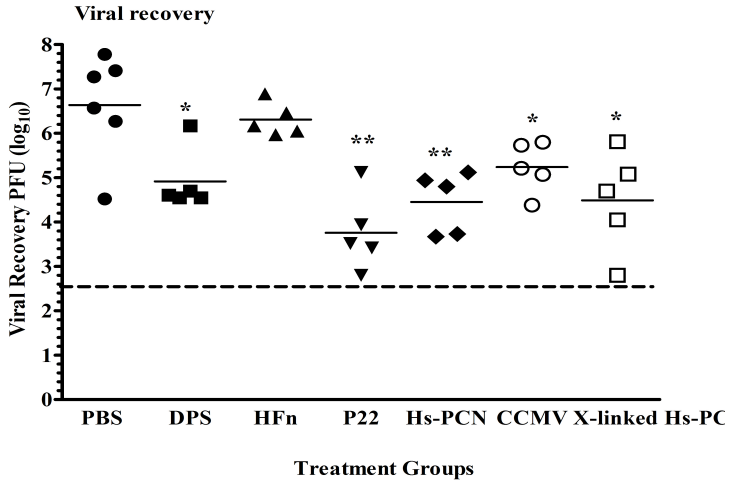


Figure 3.12: Viral recovery from mice given multiple PCN
Viral recovery from the lungs of mice that were treated with different PCN. P22 had the least viral recovery while sHsp (native and cross-linked) were slightly higher.

not all PCN provide the same amount of protection and do not produce iBALT with the same strength or frequency (figure 3.14). While each of the PCN that we tested appeared to provide some protection, the protection was not as robust as that seen in the sHsp or the P22 PCN (figure 3.11 and 3.12). An organic particle, the denrimer, with the same particulate size as sHsp, has no significant increase of protection over the control group (figure 3.10 and 3.11) and also showed no iBALT production in histology (figure 3.14). Surprisingly, unlike the externally cross-linked sHsp the internally cross-linked sHsp showed significant protection from influenza (figure 3.11 and 3.12). While the internally cross-linked sHsp did not lose much weight, the iBALT formation did not appear as robust as those formed in native sHsp (figure 3.14). While viral recovery in the cross-linked sHsp was on the same order of magnitude as that of native sHsp (figure 3.12), the influenza specific IgG were considerably lower (figure 3.13). This Suggests that while the internally cross-linked sHsp may be able to provide protection, it does not appear to facilitate the same extent of viral specific IgG

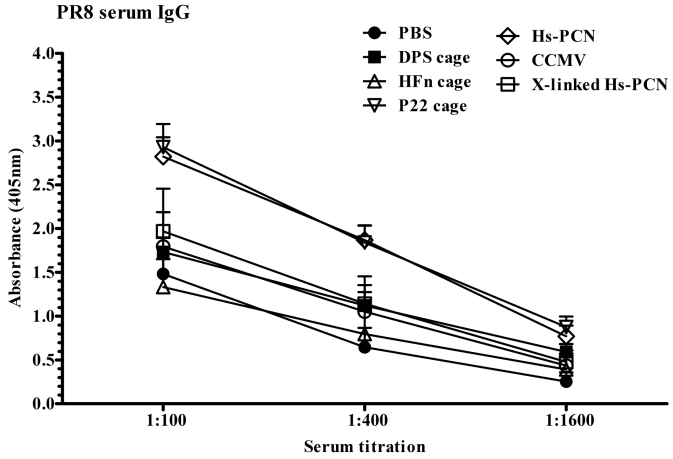


Figure 3.13: Influenza specific antibodies in mice given multiple PCN
PR8 specific serum IgG were higher in native sHsp and P22. Interestingly, they were not significantly different in any of the other cages.

seen that is seen with native sHsp. Interestingly, the only PCN that appear to enhance viral specific IgG in mice are sHsp and P22. Treatment with the other PCN does not appear to enhance the viral specific IgG response beyond that of control (figure 3.12).

The data presented above clearly indicate that sHsp is not the only PCN that can elicit a strong iBALT response in mice: P22 can also elicit a robust iBALT response providing protection form influenza. Those mice that were treated with other PCN did not have the same influenza specific IgG response that was associated with sHsp and P22. This may be because the iBALT that are produced with these PCN are not as robust as those produced with P22 and sHsp. Of notable relevance is that lung damage studies were not performed on any of the PCNs used above. Thus, although P22 appears to provide protection it is unclear if this iBALT response results in an increase in inflammation that may cause significant damage to the lungs at this time. However, P22 has the potential to become an outstanding platform for this project because of i) the capability to do *in vivo* selection and ii) co-assembly with other proteins has been accomplished. Using P22 for co-assembly will allow the attachment of a virus specific protein on the interior of the cage (i.e. nucleoprotein). This cage can be delivered to the lung. When processed the protein may be released and presented by antigen presenting cells where a memory response can be made. It was expected that if structural dynamics had a critical role in the formation of iBALT an internally cross-linked cage would have significantly less effect on iBALT production and protection. However SLS shows there may be a small

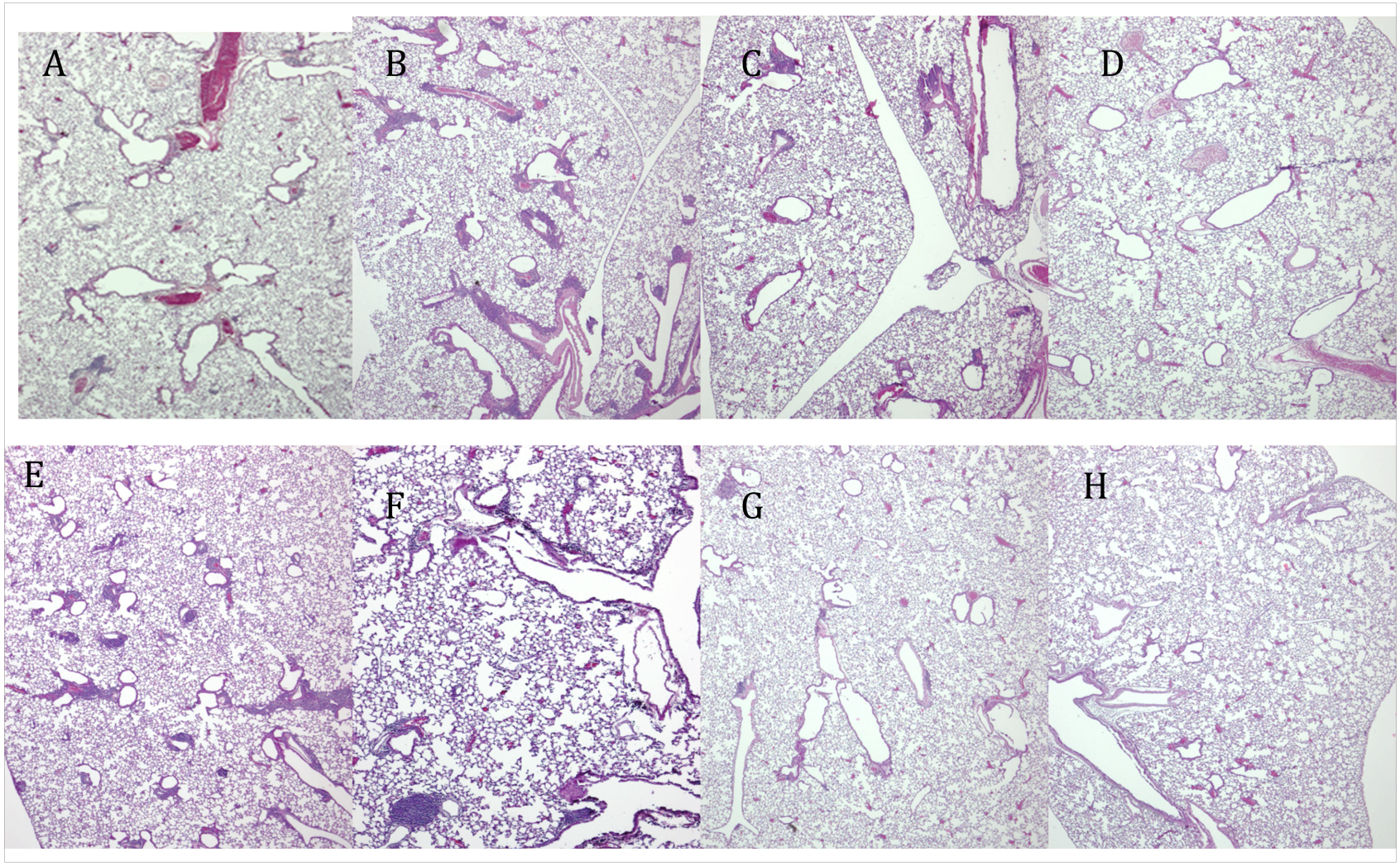


Figure 3.14: Histology for multiple cages
Lung histology pictures for mice that have been treated with 5 doses of cage A) Cross-linked sHsp B) DPS C) CCMV D) PBS E) sHsp F) P22 G) HFn H) dendrimer

amount of subunit exchange in the internally cross-linked cage thus allowing for some structural dynamics. This small amount of dynamics may play a role in the iBALT formation for the internally cross-linked sHsp. Interestingly, P22 has also been shown to undergo subunit exchange. Although this exchange is on a slower time scale than that in sHsp, structural dynamics may still play a role in iBALT formation.

Dose Response Studies

When drugs are developed it is critical to determine what quantity of drug needs to be delivered with maximum efficiency and minimum side effects. Although it has been shown that iBALT will begin to form in the lung with only one dose of 100μg of sHsp, these iBALT are not well developed and do not occur with great frequency. However, five doses over a two-week period appear to produce the most effective iBALT needed to provide the desired protection. To this point it is unknown what amount of protein needs to be delivered within the five doses to elicit the strongest response. In order to test the dose-dependence of PCN on i) iBALT production and ii) protection against viral infection, different amounts of cage were delivered to separate groups of mice.

Mice were treated with decreasing doses of PCN from 100μg to 0.5μg per dose. After five treatments one mouse was taken from each group to perform histology. Mice were then inoculated with 1500 PFU of PR8 and weighed daily to determine the percent body weight lost. Seven days post infection mice were

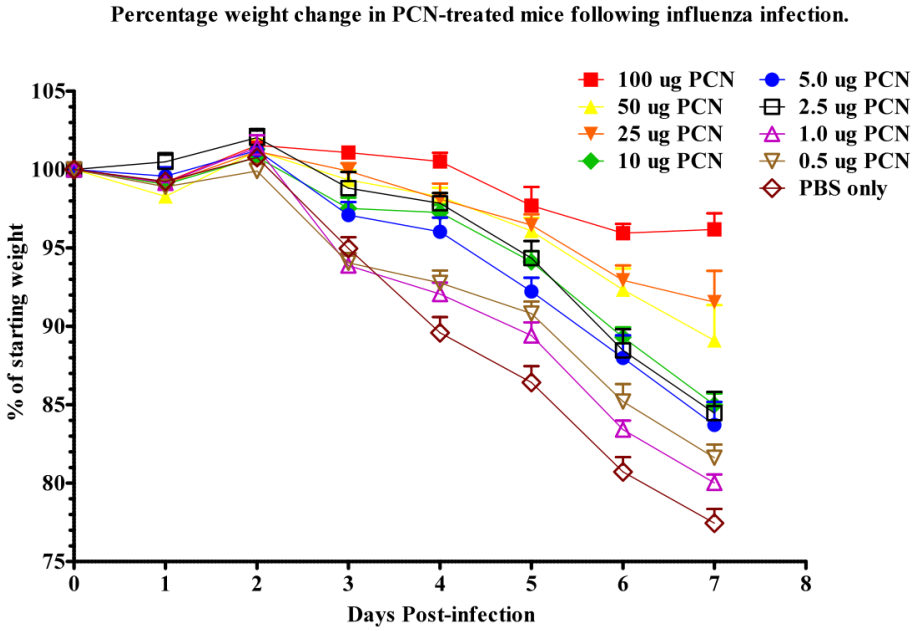
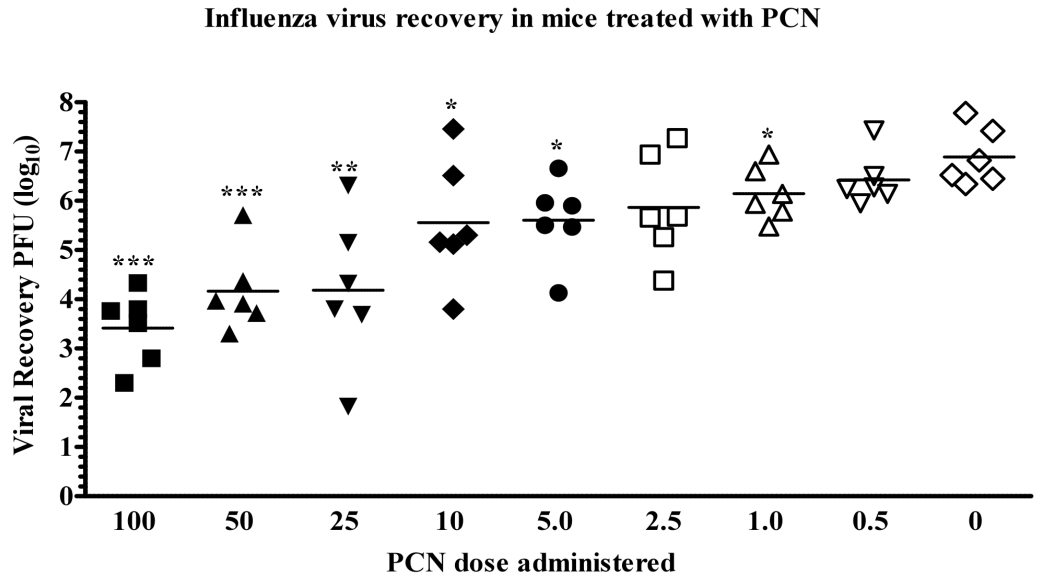


Figure 3.15: Percent weight lose for mice treated with differing amounts of sHsp
Naïve mice were treated with a decreasing amount of PCN. A robust dose dependency is evident. 10µg is the baseline dose where there is a significant loss in protection.



***, P<0.0001; **, P<0.005: *, P<0.05 relative to 0 ug PCN dose.

Figure 3.16: Viral recovery for mice treated with differing amounts of sHsp
Viral recovery from the lungs of mice treated with differing amounts of PCN. The 10µg baseline where protection is lost is evident.

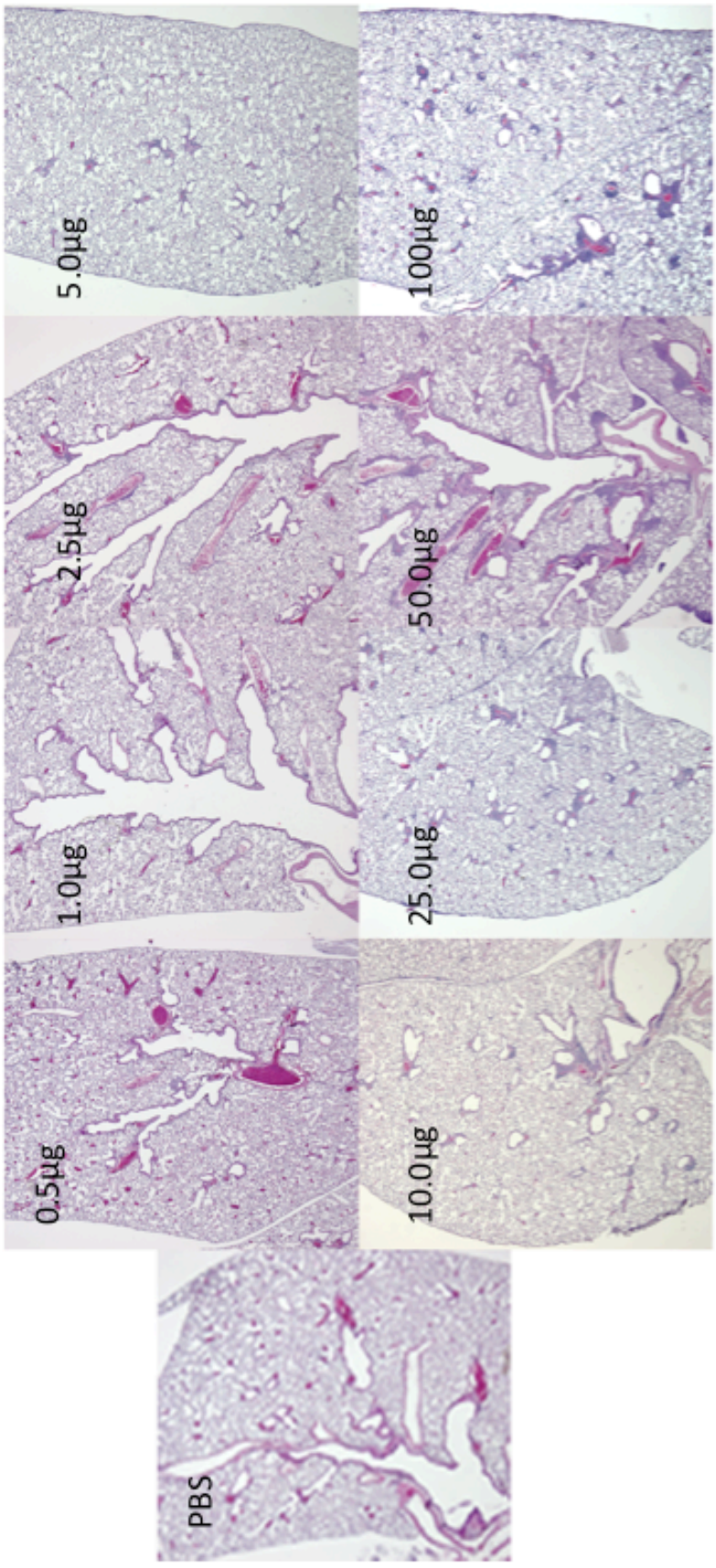


Figure 3.17: Histology for mice treated with differing amounts of sHsp
Histology images showing the increase in iBALT as sHsp dosage increases.

sacrificed and the lungs were extracted for viral recovery. BALF and serum were collected to determine the amount of PR8 specific antibodies.

Protection against influenza diminished with decreasing doses of PCN, showing a significant dose response to diminishing amounts of cage delivered (figure 3.15). There is also greater viral recovery as the dose decreases (figure 3.16). Histology also shows that as the dose decreases iBALT formations appear smaller and less frequent (figure 3.17) Below a dose of 10μg there was no significant change in the protection provided by the cage. If genetic and chemical modifications are to be tested for efficacy 10μg is the base line dose that should be used in order to observe the most effective modifications.

Testing For iBALT Response In Other Animal Models

Mice are often the first species that a potential drug is tested in because they are inexpensive to purchase and house. A number of different knockout mice are available for purchase and this can aid in determining the mechanism of the reaction and other possible side effects. Once the response has been tested and proven effective in mice it must be tested in different mammals. A specific animal is chosen for traits that resemble those of a human or traits that may provide a better indication of the strength and mechanism of the drug in question. Ferrets are commonly used to monitor influenza and potential drugs to treating influenza infections because they are extremely susceptible to influenza infections. Initial studies were done in mice. However, this used a modified

influenza strain. In order to test these effects in a more appropriate model, ferrets were subjected to the same pretreatment and infection regimens.

To date a suitable experimental protocol to effectively monitor protection from influenza in ferrets has not been developed. Currently, iBALT has been formed in the lungs of ferrets by intratracheal delivery of 12mg of PCN in 3mL of solution (figure 3.19). These iBALT structures appear to have some protective qualities to the ferret (figure 3.18). This protection has not been fully explored and in order to determine if this is a viable protective strategy more work must be accomplished.

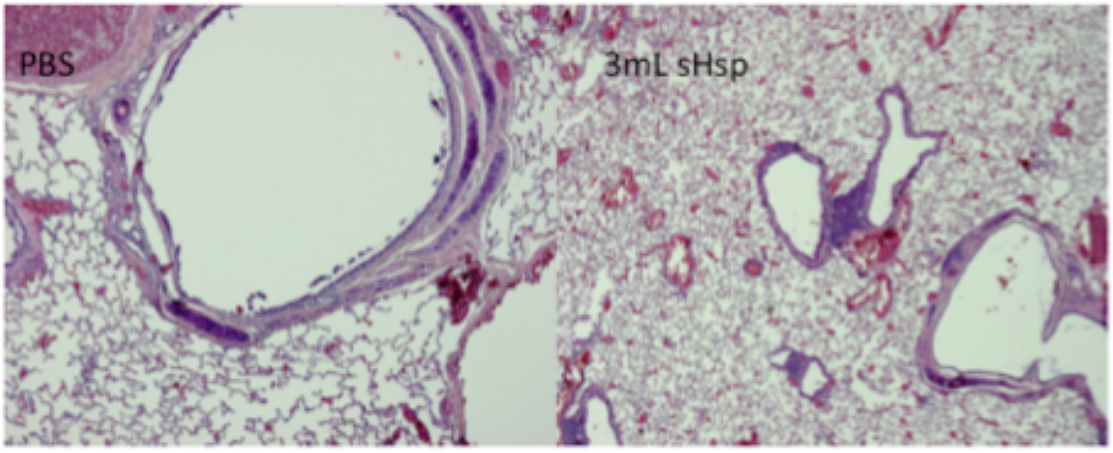


Figure 3.18: Histology for ferrets treated with sHsp
Histology images from ferret lungs showing the presence of iBALT in those treated with sHsp

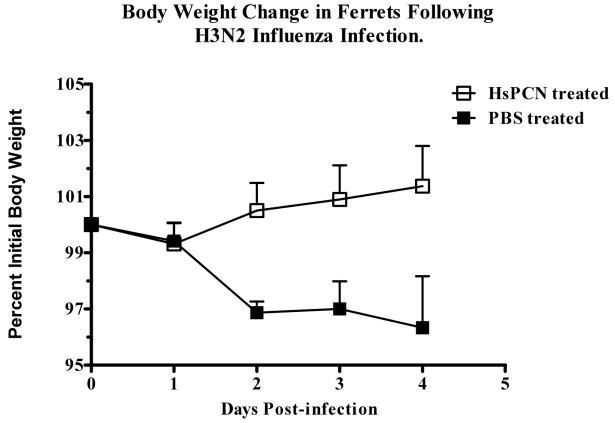


Figure 3.19: Percent weight loss in ferrets treated with sHsp
Naïve ferrets were treated with PCN followed by H3N2 influenza. Mice treated with PCN showed significant weight gain while the control ferrets lost some weight indicating an infection.

Conclusions

The mechanism for iBALT formation is poorly understood. The work presented here represents a small but significant step in deciphering the mechanism of formation. It is shown that sHsp that has been internally stabilized by covalent cross-linking induces iBALT that confer protection from influenza in mice. However, there no virus-specific IgG are detected in these mice and the iBALT formations are smaller and less frequent compared to mice treated with unmodified sHsp. This data illustrates that by stabilizing the PCN the iBALT response is attenuated suggesting that the antigenic response has been altered. Due to its more dynamic nature, the sHsp may be able to be processed faster and more completely by immune cells in the lung producing this robust response. Also presented above, is data that clearly demonstrates that iBALT can be formed with multiple PCN including bacteriophage P22 and that these PCN

provide protection from some viruses. While not all PCN are capable of producing iBALT to the same extent there are extremely promising qualities to those PCN that can produce iBALT. P22 is a promising platform for use in the production of iBALT because of its large size and ability to encapsulate cargo including viral peptides or proteins. Using this technique it may be possible to encapsulate viral proteins and possible inducing immunological memory to viral pathogens in addition to short-term protection. It has also been shown above that iBALT can be produced in other species with the sHsp PCN and that this iBALT provides protection against influenza. This has a established PCN-induced protection as a viable treatment in a more relevant model moving this prophylaxis towards clinical studies.

REFERENCES CITED

1. Parent, K.N., et al., *P22 Coat Protein Structures Reveal a Novel Mechanism for Capsid Maturation: Stability without Auxiliary Proteins or Chemical Crosslinks.* Structure. **18**(3): p. 390-401.

2. Kirksey, S.E.J., M., *The Multispecies Sallon.* http://www.skyhighway.com/~multispecies/about.html, 2006.

3. Boonyaratanakornkit, B.C., D.S.C, *Chemical Engineering, G. Vrodoljak.* Electron microscope lab, University of California Berkeley, 2006.

4. Snyder, J.C., et al., *Viruses of hyperthermophilic Archaea.* Research in Microbiology, 2003. **154**(7): p. 474-482.

5. Rice, G., et al., *Viruses from extreme thermal environments.* Proceedings of the National Academy of Sciences of the United States of America, 2001. **98**(23): p. 13341-13345.

6. Rice, G., et al., *The structure of a thermophilic archaeal virus shows a double-stranded DNA viral capsid type that spans all domains of life.* Proceedings of the National Academy of Sciences of the United States of America, 2004. **101**(20): p. 7716-7720.

7. Bath, C. and M.L. Dyall-Smith, *His1, an archaeal virus of the Fuselloviridae family that infects Haloarcula hispanica.* J Virol, 1998. **72**(11): p. 9392-5.

8. Bize, A., et al., *Viruses in acidic geothermal environments of the Kamchatka Peninsula.* Res Microbiol, 2008. **159**(5): p. 358-66.

9. Dyall-Smith, M., S.L. Tang, and C. Bath, *Haloarchaeal viruses: how diverse are they?* Res Microbiol, 2003. **154**(4): p. 309-13.

10. Pfister, P., et al., *Molecular analysis of Methanobacterium phage psiM2.* Mol Microbiol, 1998. **30**(2): p. 233-44.

11. Porter, K., B.E. Russ, and M.L. Dyall-Smith, *Virus-host interactions in salt lakes.* Curr Opin Microbiol, 2007. **10**(4): p. 418-24.

12. Prangishvili, D., P. Forterre, and R.A. Garrett, *Viruses of the Archaea: a unifying view.* Nat Rev Microbiol, 2006. **4**(11): p. 837-48.

13. Prangishvili, D., R.A. Garrett, and E.V. Koonin, *Evolutionary genomics of archaeal viruses: unique viral genomes in the third domain of life.* Virus Res, 2006. **117**(1): p. 52-67.

14. Prangishvili, D., K. Stedman, and W. Zillig, *Viruses of the extremely thermophilic archaeon Sulfolobus.* Trends Microbiol, 2001. **9**(1): p. 39-43.

15. Rachel, R., et al., *Remarkable morphological diversity of viruses and virus-like particles in hot terrestrial environments.* Arch Virol, 2002. **147**(12): p. 2419-29.

16. Rice, G., et al., *Viruses from extreme thermal environments.* Proc Natl Acad Sci U S A, 2001. **98**(23): p. 13341-5.

17. Smith, D.R., et al., *Complete genome sequence of Methanobacterium thermoautotrophicum deltaH: functional analysis and comparative genomics.* J Bacteriol, 1997. **179**(22): p. 7135-55.

18. Kim, R., et al., *Small heat shock protein of Methanococcus jannaschii, a hyperthermophile.* Proceedings of the National Academy of Sciences of the United States of America, 1998. **95**(16): p. 9129-9133.

19. Matias, P.M., et al., *Crystallization and preliminary X-ray characterization of a ferritin from the hyperthermophilic archaeon and anaerobe Pyrococcus furiosus.* Acta Crystallographica Section F-Structural Biology and Crystallization Communications, 2005. **61**: p. 503-506.

20. Kim, K.K., R. Kim, and S.H. Kim, *Crystal structure of a small heat-shock protein.* Nature, 1998. **394**(6693): p. 595-599.

21. Speir, J.A., et al., *STRUCTURES OF THE NATIVE AND SWOLLEN FORMS OF COWPEA CHLOROTIC MOTTLE VIRUS DETERMINED BY*

X-RAY CRYSTALLOGRAPHY AND CRYOELECTRON MICROSCOPY. Structure, 1995. **3**(1): p. 63-78.

22. Lander, G.C., et al., *The structure of an infectious P22 virion shows the signal for headful DNA packaging.* Science, 2006. **312**(5781): p. 1791-1795.

23. Masuda, T., et al., *The universal mechanism for iron translocation to the ferroxidase site in ferritin, which is mediated by the well conserved transit site.* Biochemical and Biophysical Research Communications, 2010. **400**(1): p. 94-99.

24. Chen, D.H., et al., *Structural basis for scaffolding-mediated assembly and maturation of a dsDNA virus.* Proceedings of the National Academy of Sciences of the United States of America, 2011. **108**(4): p. 1355-1360.

25. Uchida, M., et al., *Biological containers: Protein cages as multifunctional nanoplatforms.* Advanced Materials, 2007. **19**(8): p. 1025-1042.

26. Kumer, P.S., M. Karthikeyan, S., *Crystal structure analysis of icosahedral lumazine synthase from Salmonella typhimurium, an antibacterial drug target.* Acta Crystallography, 2011. **Sect D.**(67): p. 131-139.

27. Allen, M., et al., *Protein cage constrained synthesis of ferrimagnetic iron oxide nanoparticles.* Advanced Materials, 2002. **14**(21): p. 1562-+.

28. Allen, M., et al., *Constrained synthesis of cobalt oxide nanomaterials in the 12-subunit protein cage from Listeria innocua.* Inorganic Chemistry, 2003. **42**(20): p. 6300-6305.

29. Bulte, J.W.M., et al., *MAGNETOFERRITIN - CHARACTERIZATION OF A NOVEL SUPERPARAMAGNETIC MR CONTRAST AGENT.* Jmri-Journal of Magnetic Resonance Imaging, 1994. **4**(3): p. 497-505.

30. Chatterji, A., et al., *Cowpea mosaic virus: From the presentation of antigenic peptides to the display of active biomaterials.* Intervirology, 2002. **45**(4-6): p. 362-370.

31. Chatterji, A., et al., *Chemical conjugation of heterologous proteins on the surface of cowpea mosaic virus.* Bioconjugate Chemistry, 2004. **15**(4): p. 807-813.

32. Douglas, T. and V.T. Stark, *Nanophase cobalt oxyhydroxide mineral synthesized within the protein cage of ferritin.* Inorganic Chemistry, 2000. **39**(8): p. 1828-1830.

33. Flenniken, M.L., et al., *Selective attachment and release of a chemotherapeutic agent from the interior of a protein cage architecture.* Chemical Communications, 2005(4): p. 447-449.

34. Flenniken, M.L., et al., *A Library of Protein Cage Architectures as Nanomaterials.* Viruses and Nanotechnology, 2009. **327**: p. 71-93.

35. Flenniken, M.L., et al., *The small heat shock protein cage from Methanococcus jannaschii is a versatile nanoscale platform for genetic and chemical modification.* Nano Letters, 2003. **3**(11): p. 1573-1576.

36. Gillitzer, E., et al., *Chemical modification of a viral cage for multivalent presentation.* Chemical Communications, 2002(20): p. 2390-2391.

37. Liepold, L.O., et al., *Structural transitions in Cowpea chlorotic mottle virus (CCMV).* Physical Biology, 2005. **2**(4): p. S166-S172.

38. Varpness, Z., et al., *Biomimetic synthesis of a H-2 catalyst using a protein cage architecture.* Nano Letters, 2005. **5**(11): p. 2306-2309.

39. Allen, M.J., et al., *Cellular delivery of MRI contrast agents.* Chemistry and Biology, 2004. **11**(3): p. 301-307.

40. Douglas, T. and M. Young, *Virus particles as templates for materials synthesis.* Advanced Materials, 1999. ***11***: p. *679-681*.

41. Flenniken, M.L., et al., *Selective attachment and release of a chemotherapeutic agent from the interior of a protein cage architecture.* Chem Commun (Camb), 2005(4): p. 447-9.

42. Hikono, T., et al., *Electron confinement in a metal nanodot monolayer embedded in silicon dioxide produced using ferritin protein.* Applied Physics Letters, 2006. **88**(2).

43. Liepold, L., et al., *Viral capsids as MRI contrast agents.* Magn Reson Med, 2007. **58**(5): p. 871-9.

44. Liepold, L.O., et al., *Supramolecular Protein Cage Composite MR Contrast Agents with Extremely Efficient Relaxivity Properties.* Nano Letters, 2009.

45. Raja, K.S., Q. Wang, and M.G. Finn, *Icosahedral virus particles as polyvalent carbohydrate display platforms.* Chembiochem, 2003. **4**(12): p. 1348-51.

46. Schlick, T.L., et al., *Dual-surface modification of the tobacco mosaic virus.* Journal of the American Chemical Society, 2005. **127**(11): p. 3718-3723.

47. Wang, Q., et al., *Bioconjugation by copper(I)-catalyzed azide-alkyne [3+2] cycloaddition.* Journal of the American Chemical Society, 2003. **125**(11): p. 3192-3193.

48. Wang, Q., et al., *Natural supramolecular building blocks: Wild-type cowpea mosaic virus.* Chemistry and Biology, 2002. **9**(7): p. 805-811.

49. Wang, Q., et al., *Natural supramolecular building blocks: Cysteine-added mutants of cowpea mosaic virus.* Chemistry and Biology, 2002. **9**(7): p. 813-819.

50. Wang, Q., et al., *Icosahedral virus particles as addressable nanoscale building blocks.* Angewandte Chemie-International Edition, 2002. **41**(3): p. 459-462.

51. Gauss, G.H., et al., *Structure of the DPS-Like Protein from Sulfolobus solfataricus Reveals a Bacterioferritin-Like Dimetal Binding Site within a DPS-Like Dodecameric Assembly*. 2006. p. 10815-10827.

52. Toshiro Kitagawa, H.K., Masaki Uchida, Monica M. Dua, Yasunori Iida, Ronald L. Dalman, Trevor Douglas, and Michael V. McConnell, *RGD-Conjugated Human Ferritin Nanoparticles for Imaging Vascular Inflammation and Angiogenesis in Experimental Carotid and Aortic Disease.* Molecular Imaging and Biology, 2011. **Submitted**.

53. Ilari, A., et al., *The unusual intersubunit ferroxidase center of Listeria innocua Dps is required for hydrogen peroxide detoxification but not for iron uptake. A study with site-specific mutants.* Biochemistry, 2005. **44**(15): p. 5579-5587.

54. Jones, W.J., et al., *METHANOCOCCUS-JANNASCHII SP-NOV, AN EXTREMELY THERMOPHILIC METHANOGEN FROM A SUBMARINE HYDROTHERMAL VENT.* Archives of Microbiology, 1983. **136**(4): p. 254-261.

55. Bult, C.J., et al., *Complete genome sequence of the methanogenic archaeon, Methanococcus jannaschii.* Science, 1996. **273**(5278): p. 1058-1073.

56. Kim, K.K., et al., *Purification, crystallization, and preliminary x-ray crystallographic data analysis of small heat shock protein homolog from Methanococcus jannaschii, a hyperthermophile.* Journal of Structural Biology, 1998. **121**(1): p. 76-80.

57. Kim, R., et al., *On the mechanism of chaperone activity of the small heat-shock protein of Methanococcus jannaschii.* Proceedings of the National Academy of Sciences of the United States of America, 2003. **100**(14): p. 8151-8155.

58. Haley, D.A., et al., *Small heat-shock protein structures reveal a continuum from symmetric to variable assemblies.* Journal of Molecular Biology, 2000. **298**(2): p. 261-272.

59. Bova, M.P., et al., *Subunit exchange of alpha A-crystallin.* Journal of Biological Chemistry, 1997. **272**(47): p. 29511-29517.

60. Fu, X.M., et al., *A dual role for the N-terminal region of Mycobacterium tuberculosis Hsp16.3 in self-oligomerization and binding denaturing*

substrate proteins. Journal of Biological Chemistry, 2005. **280**(8): p. 6337-6348.

61. Brady, J.P., et al., *Targeted disruption of the mouse alpha A-crystallin gene induces cataract and cytoplasmic inclusion bodies containing the small heat shock protein alpha B-crystallin.* Proceedings of the National Academy of Sciences of the United States of America, 1997. **94**(3): p. 884-889.

62. Bova, M.P., et al., *Subunit exchange, conformational stability, and chaperone-like function of the small heat shock protein 16.5 from Methanococcus jannaschii.* Journal of Biological Chemistry, 2002. **277**(41): p. 38468-38475.

63. Klem, M.T., et al., *Bio-inspired synthesis of protein-encapsulated CoPt nanoparticles.* Advanced Functional Materials, 2005. **15**(9): p. 1489-1494.

64. Abedin, M.J., et al., *Synthesis of a cross-linked branched polymer network in the interior of a protein cage.* J Am Chem Soc, 2009. **131**(12): p. 4346-54.

65. Murphy, R.F., S. Powers, and C.R. Cantor, *ENDOSOME PH MEASURED IN SINGLE CELLS BY DUAL FLUORESCENCE FLOW-CYTOMETRY - RAPID ACIDIFICATION OF INSULIN TO PH-6.* Journal of Cell Biology, 1984. **98**(5): p. 1757-1762.

66. Wiley, J.A., et al., *Inducible Bronchus-Associated Lymphoid Tissue Elicited by a Protein Cage Nanoparticle Enhances Protection in Mice against Diverse Respiratory Viruses.* Plos One, 2009. **4**(9).

67. Wiley, J.A. and A.G. Harmsen, *Pneumocystis infection enhances antibody-mediated resistance to a subsequent influenza infection.* Journal of Immunology, 2008. **180**(8): p. 5613-5624.

68. Randall, T.D., *Bronchus-associated lymphoid tissue (BALT) structure and function.* Adv Immunol. **107**: p. 187-241.

69. Moyron-Quiroz, J.E., et al., *Role of inducible bronchus associated lymphoid tissue (iBALT) in respiratory immunity.* Nature Medicine, 2004. **10**(9): p. 927-934.

70. Bradley, D.E., *ULTRASTRUCTURE OF BACTERIOPHAGES AND BACTERIOCINS.* Bacteriological Reviews, 1967. **31**(4): p. 230-&.

71. Iwashita, S. and Kanegasa.S, *SMOOTH SPECIFIC PHAGE ADSORPTION - ENDORHAMNOSIDASE ACTIVITY OF TAIL PARTS OF P22.* Biochemical and Biophysical Research Communications, 1973. **55**(2): p. 403-409.

72. Israel, V., H. Rosen, and M. Levine, *BINDING OF BACTERIOPHAGE-P22 TAIL PARTS TO CELLS.* Journal of Virology, 1972. **10**(6): p. 1152-1158.

73. Susskind, M.M. and D. Botstein, *MOLECULAR GENETICS OF BACTERIOPHAGE-P22.* Microbiological Reviews, 1978. **42**(2): p. 385-413.

74. Jiang, W., et al., *Coat protein fold and maturation transition of bacteriophage P22 seen at subnanometer resolutions.* Nature Structural Biology, 2003. **10**(2): p. 131.

75. Zhang, Z.X., et al., *Visualization of the maturation transition in bacteriophage P22 by electron cryomicroscopy.* Journal of Molecular Biology, 2000. **297**(3): p. 615-626.

76. ThumanCommike, P.A., et al., *Three-dimensional structure of scaffolding-containing phage P22 procapsids by electron cryo-microscopy.* Journal of Molecular Biology, 1996. **260**(1): p. 85-98.

77. Johnson, J.E. and W. Chiu, *DNA packaging and delivery machines in tailed bacteriophages.* Current Opinion in Structural Biology, 2007. **17**(2): p. 237-243.

78. Jackson, E.N., F. Laski, and C. Andres, *BACTERIOPHAGE P22 MUTANTS THAT ALTER THE SPECIFICITY OF DNA PACKAGING.* Journal of Molecular Biology, 1982. **154**(4): p. 551-563.

79. Casjens, S. and W.M. Huang, *INITIATION OF SEQUENTIAL PACKAGING OF BACTERIOPHAGE-P22 DNA.* Journal of Molecular Biology, 1982. **157**(2): p. 287-298.

80. Fuller, D.N., et al., *Measurements of single DNA molecule packaging dynamics in bacteriophage lambda reveal high forces, high motor processivity, and capsid transformations.* Journal of Molecular Biology, 2007. **373**: p. 1113-1122.

81. Smith, D.E., et al., *The bacteriophage phi 29 portal motor can package DNA against a large internal force.* Nature, 2001. **413**(6857): p. 748-752.

82. Earnshaw, W., S. Casjens, and S.C. Harrison, *Assembly of the head of bacteriophage P22: X-ray diffraction from heads, proheads and related structures.* Journal of Molecular Biology, 1976. **104**(2): p. 387-410.

83. Kang, S. and P.E. Prevelige, *Domain Study of Bacteriophage P22 Coat Protein and Characterization of the Capsid Lattice Transformation by Hydrogen/Deuterium Exchange.* Journal of Molecular Biology, 2005. **347**(5): p. 935-948.

84. Parent, K.N., et al., *Cryo-reconstructions of P22 polyheads suggest that phage assembly is nucleated by trimeric interactions among coat proteins.* Physical Biology. **7**(4): p. 14.

85. Teschke, C.M., A. McGough, and P.A. Thuman-Commike, *Penton Release from P22 Heat-Expanded Capsids Suggests Importance of Stabilizing Penton-Hexon Interactions during Capsid Maturation.* Biophysical Journal, 2003. **84**(4): p. 2585-2592.

86. Tuma, R. and P.E. Prevelige, *Structural transitions in the scaffolding and coat.* Biochemistry, 1996. **35**(14): p. 4619.

87. Parker, M.H., S. Casjens, and P.E. Prevelige Jr, *Functional domains of bacteriophage P22 scaffolding protein.* Journal of Molecular Biology, 1998. **281**(1): p. 69-79.

88. Parker, M.H., C.G. Brouillette, and P.E. Prevelige Jr, *Kinetic and Calorimetric Evidence for Two Distinct Scaffolding Protein Binding Populations within.* Biochemistry, 2001. **40**(30): p. 8962.

89. Greene, B. and J. King, *BINDING OF SCAFFOLDING SUBUNITS WITHIN THE P22 PROCAPSID LATTICE.* Virology, 1994. **205**(1): p. 188-197.

90. Miller, I.A., et al., *BACTERIOPHAGE-P22 AS A VEHICLE FOR TRANSDUCING COSMID GENE BANKS BETWEEN SMOOTH STRAINS OF SALMONELLA-TYPHIMURIUM - USE IN IDENTIFYING A ROLE FOR AROD IN ATTENUATING VIRULENT SALMONELLA STRAINS.* Molecular & General Genetics, 1989. **215**(2): p. 312-316.

91. Kang, S., et al., *Implementation of P22 Viral Capsids as Nanoplatforms.* Biomacromolecules. **11**(10): p. 2804-2809.

92. Uchida M., K.S., Lucon J., O'Neil A., LaFrance B., Prevelige P. and Douglas T., *Encapsulation of a small protein cargo inside of P22 viral capsid via metal-ligand coordination bond.* In preparation, 2011.

93. Alison O'Neil, C.R., Benjamin Johnson, Peter E. Prevelige, and Trevor Douglas, *Genetically Programmed in vivo Packaging and Controlled Release of Protein Cargo*
from Bacteriophage P22. Journal of American Chemical society, 2011. **Submitted**.

94. Alison O'Neil, C.R., Benjamin Johnson, Peter E. Prevelige, and Trevor Douglas, *P22 Nano-reactors: High copy number delivers high efficiency.* In preparation, 2011.

95. Zlotnick, A., et al., *Mechanism of capsid assembly for an icosahedral plant virus.* Virology, 2000. **277**(2): p. 450-456.

96. Johnson, J.E. and J.A. Speir, *Quasi-equivalent viruses: A paradigm for protein assemblies.* Journal of Molecular Biology, 1997. **269**(5): p. 665-675.

97. Bancroft, J.B., et al., *PROPERTIES OF COWPEA CHLOROTIC MOTTLE VIRUS ITS PROTEIN AND NUCLEIC ACID.* Virology, 1968. **34**(2): p. 224-&.

98. Fox, J.M., et al., *Analysis of a salt stable mutant of cowpea chlorotic mottle virus.* Virology, 1996. **222**(1): p. 115-122.

99. Arosio, P. and S. Levi, *Ferritin, iron homeostasis, and oxidative damage.* Free Radical Biology and Medicine, 2002. **33**(4): p. 457-463.

100. Harrison, P.M. and P. Arosio, *Ferritins: Molecular properties, iron storage function and cellular regulation.* Biochimica Et Biophysica Acta-Bioenergetics, 1996. **1275**(3): p. 161-203.

101. Harrison, P.M., et al., *The structure and function of ferritin.* Ciba Found Symp, 1976(51): p. 19-40.

102. Wang, Z.M., et al., *Structure of human ferritin L chain.* Acta Crystallographica Section D-Biological Crystallography, 2006. **62**: p. 800-806.

103. Klem, M.T., et al., *Synthetic control over magnetic moment and exchange bias in all-oxide materials encapsulated within a spherical protein cage.* Journal of the American Chemical Society, 2007. **129**(1): p. 197-201.

104. Yamashita, I., J. Hayashi, and M. Hara, *Bio-template synthesis of uniform CdSe nanoparticles using cage-shaped protein, apoferritin.* Chemistry Letters, 2004. **33**(9): p. 1158-1159.

105. Ensign, D., M. Young, and T. Douglas, *Photocatalytic synthesis of copper colloids from Cu(II) by the ferrihydrite core of ferritin.* Inorganic Chemistry, 2004. **43**(11): p. 3441-3446.

106. Okuda, M., et al., *Fabrication of nickel and chromium nanoparticles using the protein cage of apoferritin.* Biotechnology and Bioengineering, 2003. **84**(2): p. 187-194.

107. Grant, R.A., et al., *The crystal structure of Dps, a ferritin homolog that binds and protects DNA.* Nature Structural Biology, 1998. **5**(4): p. 294-303.

108. Bozzi, M., et al., *A novel non-heme iron-binding ferritin related to the DNA-binding proteins of the Dps family in Listeria innocua.* Journal Of Biological Chemistry, 1997. **272**(6): p. 3259-3265.

109. Ilari, A., et al., *The dodecameric ferritin from Listeria innocua contains a novel intersubunit iron-binding site.* Nature Structural Biology, 2000. **7**(1): p. 38-43.

110. Stefanini, S., et al., *Incorporation of iron by the unusual dodecameric ferritin from Listeria innocua.* Biochemical Journal, 1999. **338**: p. 71-75.

111. Su, M.H., et al., *The so-called Listeria innocua ferritin is a Dps protein. Iron incorporation, detoxification, and DNA protection properties.* Biochemistry, 2005. **44**(15): p. 5572-5578.

112. Wiedenheft, B., et al., *An archaeal antioxidant: Characterization of a Dps-like protein from Sulfolobus solfataricus.* Proceedings of the National Academy of Sciences of the United States of America, 2005. **102**(30): p. 10551-10556.

113. Fischer, M. and F. Vogtle, *Dendrimers: From design to application - A progress report.* Angewandte Chemie-International Edition, 1999. **38**(7): p. 885-905.

114. Antoni, P., et al., *Bifunctional Dendrimers: From Robust Synthesis and Accelerated One-Pot Postfunctionalization Strategy to Potential Applications.* Angewandte Chemie-International Edition, 2009. **48**(12): p. 2126-2130.

115. Liang, C.O. and J.M.J. Frechet, *Incorporation of functional guest molecules into an internally functionalizable dendrimer through olefin metathesis.* Macromolecules, 2005. **38**(15): p. 6276-6284.

116. Cheng, Y.Y., et al., *External electrostatic interaction versus internal encapsulation between cationic dendrimers and negatively charged drugs:*

Which contributes more to solubility enhancement of the drugs? Journal of Physical Chemistry B, 2008. **112**(30): p. 8884-8890.

117. McElhanon, J.R. and D.V. McGrath, *Toward chiral polyhydroxylated dendrimers. Preparation and chiroptical properties.* Journal of Organic Chemistry, 2000. **65**(11): p. 3525-3529.

118. Tekade, R.K., et al., *Exploring dendrimer towards dual drug delivery: pH responsive simultaneous drug-release kinetics.* Journal of Microencapsulation, 2009. **26**(4): p. 287-296.

119. Huang, J.F., et al., *Hydrophobic bronsted acid-base ionic liquids based on PAMAM dendrimers with high proton conductivity and blue photoluminescence.* Journal of the American Chemical Society, 2005. **127**(37): p. 12784-12785.

120. Grabchev, I., D. Staneva, and J.M. Chovelon, *Photophysical investigations on the sensor potential of novel, poly(propylenamine) dendrimers modified with 1,8-naphthalimide units.* Dyes and Pigments, 2010. **85**(3): p. 189-193.

121. Fu, H.L., et al., *Dendrimer/DNA complexes encapsulated functional biodegradable polymer for substrate-mediated gene delivery.* Journal of Gene Medicine, 2008. **10**(12): p. 1334-1342.

122. Douglas, T. and M. Young, *Virus particles as templates for materials synthesis.* Advanced Materials, 1999. **11**(8): p. 679-+.

123. Koo, M., et al., *Protective immunity against murine hepatitis virus (MHV) induced by intranasal or subcutaneous administration of hybrids of tobacco mosaic virus that carries an MHV epitope.* Proceedings of the National Academy of Sciences of the United States of America, 1999. **96**(14): p. 7774-7779.

124. Yusibov, V., et al., *Expression in plants and immunogenicity of plant virus-based experimental rabies vaccine.* Vaccine, 2002. **20**(25-26): p. 3155-3164.

125. Portney, N.G., et al., *Organic and inorganic nanoparticle hybrids.* Langmuir, 2005. **21**(6): p. 2098-2103.

126. Ewers, H., et al., *Single-particle tracking of murine polyoma virus-like particles on live cells and artificial membranes.* Proceedings of the National Academy of Sciences of the United States of America, 2005. **102**(42): p. 15110-15115.

127. Gleiter, S. and H. Lilie, *Cell-type specific targeting and gene expression using a variant of polyoma VP1 virus-like particles.* Biological Chemistry, 2003. **384**(2): p. 247-255.

128. Bok, K., et al., *Chimpanzees as an animal model for human norovirus infection and vaccine development.* Proceedings of the National Academy of Sciences of the United States of America, 2011. **108**(1): p. 325-330.

129. El-Kamary, S.S., et al., *Adjuvanted Intranasal Norwalk Virus-Like Particle Vaccine Elicits Antibodies and Antibody-Secreting Cells That Express Homing Receptors for Mucosal and Peripheral Lymphoid Tissues.* Journal of Infectious Diseases, 2010. **202**(11): p. 1649-1658.

130. Velasquez, L.S., et al., *An Intranasally Delivered Toll-Like Receptor 7 Agonist Elicits Robust Systemic and Mucosal Responses to Norwalk Virus-Like Particles.* Clinical and Vaccine Immunology, 2010. **17**(12): p. 1850-1858.

131. Henning, P., et al., *Tumor cell targeted gene delivery by adenovirus 5 vectors carrying knobless fibers with antibody-binding domains.* Gene Therapy, 2005. **12**(3): p. 211-224.

132. Hong, S.S., et al., *Adenovirus stripping: A versatile method to generate adenovirus vectors with new cell target specificity.* Molecular Therapy, 2003. **7**(5): p. 692-699.

133. Douglas, J.T., et al., *A system for the propagation of adenoviral vectors with genetically modified receptor specificities.* Nature Biotechnology, 1999. **17**(5): p. 470-475.

134. Hooker, J.M., E.W. Kovacs, and M.B. Francis, *Interior surface modification of bacteriophage MS2.* Journal of the American Chemical Society, 2004. **126**(12): p. 3718-3719.

135. Brown, S.D., J.D. Fiedler, and M.G. Finn, *Assembly of Hybrid Bacteriophage Q beta Virus-like Particles.* Biochemistry, 2009. **48**(47): p. 11155-11157.

136. Li, X.M., et al., *Induction of protective immunity in swine by immunization with live attenuated recombinant pseudorabies virus expressing the capsid precursor encoding regions of foot-and-mouth disease virus.* Vaccine, 2008. **26**(22): p. 2714-2722.

137. Singh, P., et al., *Canine parvovirus-like particles, a novel nanomaterial for tumor targeting.* J Nanobiotechnology, 2006. **4**: p. 2.

138. Peabody, D.S., *A viral platform for chemical modification and multivalent display.* Journal of Nanobiotechnology, 2003. **1**(5 Cited November 24, 2003).

139. Garrett R. H., G.C.H., *Biochemistry*. third ed, ed. S. Kielsica. 2007, Belmont: Thomson Brooks/cole. 1085.

140. Wyatt, P.J., *LIGHT-SCATTERING AND THE ABSOLUTE CHARACTERIZATION OF MACROMOLECULES.* Analytica Chimica Acta, 1993. **272**(1): p. 1-40.

141. Heller, W. and M. Nakagaki, *LIGHT-SCATTERING OF SPHEROIDS .1. EXTENSION OF RAYLEIGH-GANS-STEVENSON FUNCTIONS AND THEIR APPLICATION FOR MOLECULAR-WEIGHT AND SHAPE DETERMINATION AT THETA =90 DEGREES.* Journal of Chemical Physics, 1974. **60**(10): p. 3889-3895.

142. Stewart, J.Q., *Generalizations of the Rayleigh formula for molecular scattering.* Journal of the Optical Society of America and Review of Scientific Instruments, 1925. **11**(6): p. 581-597.

143. Riehl, N., *Diffusion coefficient and water content of globular protein molecules.* Hoppe-Seylers Zeitschrift Fur Physiologische Chemie, 1944. **281**: p. 73-83.

144. Thuman-Commike, P.A., et al., *Role of the scaffolding protein in P22 procapsid size determination suggested by T = 4 and T = 7 procapsid structures.* Biophysical Journal, 1998. **74**(1): p. 559-568.

145. Tang, L., et al., *Highly discriminatory binding of capsid-cementing proteins in bacteriophage L.* Structure, 2006. **14**(5): p. 837-845.

146. Gilcrease, E.B., et al., *Nucleotide sequence of the head assembly gene cluster of bacteriophage L and decoration protein characterization.* Journal of Bacteriology, 2005. **187**(6): p. 2050-2057.

147. Popa, M.P., et al., *BACTERIOPHAGE-HK97 STRUCTURE - WHOLESALE COVALENT CROSS-LINKING BETWEEN THE MAJOR HEAD SHELL SUBUNITS.* Journal of Virology, 1991. **65**(6): p. 3227-3237.

148. Yang, Q., N.K. Maluf, and C.E. Catalano, *Packaging of a Unit-Length Viral Genome: The Role of Nucleotides and the gpD Decoration Protein in Stable Nucleocapsid Assembly in Bacteriophage lambda.* Journal of Molecular Biology, 2008. **383**(5): p. 1037-1048.

149. Kindt, T.J.G., R. A. Osborne B. A., *Kuby Immunology*. 6 ed, ed. K. Ahr. 2004, New York: W.H. Freeman and Company. 574.

150. Kindt, T.J.G., R. A. Osborne B. A., *Kuby Immunology*. 6 ed, ed. K. Ahr. 2007, New York: W.H. Freeman and Company. 8-16.

151. Goodnow, C.C., *Chance encounters and organized rendezvous.* Immunological Reviews, 1997. **156**: p. 5-10.

152. Zinkernagel, R.M., et al., *Antigen localisation regulates immune responses in a dose- and time-dependent fashion: A geographical view of immune reactivity.* Immunological Reviews, 1997. **156**: p. 199-209.

153. Karrer, U., et al., *On the key role of secondary lymphoid organs in antiviral immune responses studied in alymphoplastic (aly/aly) and spleenless (Hox11(-/-)) mutant mice.* Journal of Experimental Medicine, 1997. **185**(12): p. 2157-2170.

154. Lakkis, F.G., et al., *Immunologic 'ignorance' of vascularized organ transplants in the absence of secondary lymphoid tissue.* Nature Medicine, 2000. **6**(6): p. 686-688.

155. Rennert, P.D., et al., *Essential role of lymph nodes in contact hypersensitivity revealed in lymphotoxin-alpha-deficient mice.* Journal of Experimental Medicine, 2001. **193**(11): p. 1227-1238.

156. Carragher, D.M., J. Rangel-Moreno, and T.D. Randall, *Ectopic lymphoid tissues and local immunity.* Seminars in Immunology, 2008. **20**(1): p. 26-42.

157. Park, H.S., et al., *Membranous cells in nasal-associated lymphoid tissue: A portal of entry for the respiratory mucosal pathogen group A streptococcus.* Journal of Immunology, 2003. **171**(5): p. 2532-2537.

158. GeurtsvanKessel, C.H., et al., *Dendritic cells are crucial for maintenance of tertiary lymphoid structures in the lung of influenza virus-infected mice.* Journal of Experimental Medicine, 2009. **206**(11): p. 2339-2349.

159. Aloisi, F. and R. Pujol-Borrell, *Lymphoid neogenesis in chronic inflammatory diseases.* Nature Reviews Immunology, 2006. **6**(3): p. 205-217.

160. Corr, S.C., C. Gahan, and C. Hill, *M-cells: origin, morphology and role in mucosal immunity and microbial pathogenesis.* Fems Immunology and Medical Microbiology, 2008. **52**(1): p. 2-12.

161. Kashino, S.S., et al., *Initiation of Acquired Immunity in the Lungs of Mice Lacking Lymph Nodes after Infection with Aerosolized Mycobacterium tuberculosis.* American Journal of Pathology. **176**(1): p. 198-204.

APPENDIX A

MATERIALS AND METHODS

P22 Capsid Purification

Transformed BL21 (DE3) *E. coli* were grown to an OD_{600nm} = 0.6 and then induced with 1mM IPTG. The culture was allowed to grow an additional 4 hours at 37°C with vigorous shaking. The bacteria were then centrifuged away from the media at 3700 x rpm for 15 minutes. The cell pellets were resuspended in 50mM PO_4 100mM NaCl pH 7.2 and frozen at -20°C overnight. The next day, the cell pellets were thawed and incubated with DNAse, RNAse, and lysozyme (all Sigma-Aldrich) for 30 minutes at room temperature. Cells were lysed further by sonication on ice. The cell debris was removed via centrifugation at 5000 x rpm for 45 minutes. The supernatant was then loaded on a 35% (w/v) sucrose cushion and centrifuged at 48k x rpm for 50 minutes in an ultra centrifuge (Sorval). The resulting virus pellet was resuspended in 50mM PO_4 25mM NaCl pH 7.6, spun at 17k x rpm for 20 minutes to remove and particulates and lipid. The virus was then dialyzed against the 50mM Po_4 100mM NaCl buffer overnight.

Ion Exchange Chromotagraphy

Purified Capsid was injected on a Q column after washing the column for 10 minutes with 50mM Hepes pH 8.0 (buffer A). The column was washed an additional 10 minutes after injection. A linear gradient was applied from 100% buffer A to 50% buffer A 50% 50mM Hepes 1M NaCl pH 8.0 (buffer B) over 50 minutes. A linear gradient from 50% buffer B 50% buffer A to 100% buffer B was applied over 20 minutes. The Column was washed with 100% B for 5 minutes than returned to 100% buffer A. Fractions were collected.

Native agarose gel electrophoresis

A 0.8% agrose gel was made up in 40mM Tris base 1mM EDTA (Running buffer). Samples were applied with 4X loading buffer as above with the addition of 20% sucrose and bromophenyl blue. The gel was run for 3 hours in running buffer and protein was detected by coomassie staining.

Dynamic light scattering

Purified capsid was spun for 5 minutes at 16 000 x g and filter into cuvette through a 0.2µM filter. Samples were run for 5 minutes on a 90plus particle size analyzer (Brookhaven). Correlation functions were fit using dynamic light scattering software (Brookhaven) to determine molecular diameter.

Size exclusion chromatography - Multi angle light scattering

P22 capsid samples were separated by size exclusion chromatography column WTC-0200S (Wyatt Technologies). Samples were injected and the mobile phase was applied using an Agilent 1200 at a flow rate of 0.7 mLs/min. The mobile phase was 50mM phosphate 100mM NaCl 200ppm azide at pH 7.2. 25µL of sample was injected on the column and run for 30 minutes. Samples were monitored using both a UV-vis detector (Agilent) and a refractive index detector (Wyatt) to determine concentration. Multi angle light scattering was detected with a Dawn 8 (Wyatt). Average Mw and Rg was fit using a Zimm plot in Astra (Wyatt). The most important parameter in the fit is to insure that the baselines are set properly and that all peaks overlap correctly. To ensure proper fit of base line zoom in where the peak begins and ensure that all peaks overlap. To ensure a correct average Mw and Rg (assuming a monodispersed sample) select the center of the peak. If the tails of the peaks are selected Mw can be slightly off.

Analytical ultra centrifugation

Sedimentation velocity experiments were performed on an XL-A ultracentrifuge (Beckman Coulter, Fullerton, CA) using a AN-60Ti. Epon double-sector centerpieces were filled with 400 µL of a sample and a corresponding reference buffer (Tris 50mM, sodium chloride 100mM, pH7.5) and centrifuged at 23,000 rpm and at 20°C. Absorbance data were acquired at wavelength of 280nm. The collected data were analyzed and fitted using SEDFIT software. Input parameters such as the partial specific volume, buffer density and viscosity were determined using Sednterp software.

Determination of proteins by trypsin digestion

Protein concetration was determined by UV/Vis and was between 1 and 10mg/mL. 20µL of sample was dried with a speed vac at 80°C. Pellet was resuspended in 10µL freshly made 8M urea in 100mM Tris-HCl pH 8.5 and 5mM DTT. Protein was allowed resuspended for 1 hour at 60°C to ensure that the protein was completely disassembled. 30µL of 100mM Tris-HCl was added to make the final urea concentration 2M. 1/100 trypsin to protein (w/w) was added and incubated over night at 37°C. Samples were analyzied on the mass spec using ProLynx software.

Chloroform extraction

P22 PC and PC-OmpF were mixed 1:1 with chloroform in a glass vial and shaken for 5 minutes. The samples were than allowed to sit until the organic layer separated from the aqueous layer. Samples were separated with a glass

syringe and lipid presence was determined by LC-MS using a C-8 column.

Hsp Mutagenesis

Polymerase chain reaction (PCR) mediated site directed mutagenesis was employed to engineer destabilizing amino acids in the *Mj*Hsp16.5 clone (Stratagene). Complementary forward and reverse mutagenesis primers were designed to contain the two point mutations needed to change arginine to a Glutaminc acid at position 93 (R93E) of the *Mj*Hsp 9(+) 5' ATA ACT GAG AGT GAA GAA ATT ATC TAC TCA GAA ATT CCA GAA GAG G 3'. Likewise in order to make the E92K mutant, glutamic acid was changed to lysine. The *Mj*Hsp E92K mutagenesis primer sequences are as follows: (-) 5' GGA ATT TCT GAG TAG ATA ATT CTT TTA CTC TCA GTT ATC ATT AAT GG 3'. In order to make the E98K mutant, glutamic acid was changed to lysine. The *Mj*Hsp E98K mutagenesis primer sequences are as follows: (-) 5' TTC TTC CTC TTC TGG AAT TTT TGA GTA GAT AAT 3'. In order to make the K141E mutant, lysine was changed to glutaminc acid. The *Mj*Hsp K141E mutagenesis primer sequences are as follows: (-) 5' TTC AAT GTT GAT TCC TTC CTC AAT TGA GGAT TCT GCC 3'. In order to make the K142E mutant, lysine was changed to glutaminc acid. The *Mj*Hsp K142E mutagenesis primer sequences are as follows: (-) 5' TTA TTC AAT GTT GAT TCC TTC CTT AAT TGA GGA TTC TGC C 3'. *Methanococcus jannaschii* genomic DNA was obtained from the American Type Culture Collection (ATTC 43067). The gene encoding the small heat shock protein Hsp16.5 was amplified by polymerase chain reaction (PCR) with the using the above primers. The vector was transformed into XL2 Blue *E. coli* (Stratagene, LaJolla, CA) for selection. Positive colonies were grown overnight in LB + kanamycin, plasmid DNA was isolated (Eppendorf Mini Prep Kit), and inserted DNA was sequenced by an ABI 310 automated capillary sequencer using Big Dye chain termination sequence technology (Applied Bio Systems, Foster City, CA). After sequence verification, the pET-30a(+) *Mj*Hsp16.5 was subcloned into BL21(DE3) B strain *E. coli* (Novagen).

Expression and purification of sHsp

One liter cultures of *E. coli* (BL21(DE3) B strain) containing pET-30a(+) *Mj*Hsp16.5 plasmid were grown overnight in LB + kanamycin medium (37^0C, 220 rpm). Cells were harvested by centrifugation 3700xg for 20 minutes (Heraeus #3334 rotor, Sorvall Centrifuge) and re-suspended in 25 milliliters of 100mM HEPES, pH 8.0. Lysozyme and DNase were added to final concentrations of 1 mg/ml and 1 mg/L respectively. The sample was incubated for 30 minutes on ice and sonicated on ice (Branson Sonifier 250, Power 4, Duty cycle 50%, 3 x 5minutes with 3 minute intervals). Bacterial cell debris was removed *via* centrifugation for 45 minutes at 12,000xg. The supernatant was heated for 15 minutes at 60°C thereby denaturing many heat labile *E. coli* proteins. The

supernatant was centrifuged for 20 minutes at 12,000xg and then purified by gel filtration chromatography (Superose-6, Amersham-Pharmacia; Biorad Duoflow). The 16.5 kDa subunit molecular weight (*Mj*Hsp16.5) was verified by SDS poly-acrylamide gel electrophoresis (SDS-PAGE). The assembled protein was imaged by transmission electron microscopy (TEM) (LEO 912 AB) (stained with 2% uranyl acetate on formvar carbon coated grids), and analyzed by dynamic light scattering (DLS) 90 plus (Brookhaven Instruments). Protein concentration was determined by absorbance at 280 nm divided by the published extinction coefficient (9322 $M^{-1}cm^{-1}$; 0.565 $(mg/ml)^{-1}cm^{-1}$).

90° static light scattering

Samples were prepared in PBS pH 7.2 at approximately 2mg/mL. 2mL of sample was placed in a fluorescent cuvette and placed in a peltier heating/cooling cuvette holder at 25°C. A xenon arc lamp was used to light the sample and scattering was detected at 90° C using an ocean optics S2000 spectrophotometer. A full UV/Vis spectrum was taken using the Spectasuite software. Temperature was raised using the peltier heater (Quantum Northwest) to 40°C. The sample was allowed 10 mins to equilibrate to the temperature and a full UV/Vis spectrum was taken. This was repeated for 60°C, 80°C and 100°C. Scattering intensity was determined by the area under the UV/Vis curve and plotted using Igor.

General Cross-Linking Protocol.

Cross-linking reactions were carried out in a total volume of 20 ml in a buffer comprised of 50 mM sodium phosphate (pH 7.5), 100 mM NaCl, and 0.125 mM Ru(bpy)3Cl2 (Aldrich). Easily oxidized buffer components such as b-mercaptoethanol and DTT should be avoided. Protein concentrations varied depending on the experiment between 1 mg/mL. The solution was placed in a 1.7-ml Eppendorf tube positioned parallel to the beam of light from and LED (wavelength 450nm). Ammonium persulfate (APS) was added to 2.5 mM just before irradiation. In most experiments, the sample was irradiated for 10 seconds. Samples were analyzed for cross-linking by gradient SDS-PAGE gel (10-20%). Proteins were visualized by staining with Coomassie brilliant blue. Protocol adapted from Fancy et al. 1999 PNAS.

Protein digest and mass spectrometry

Protein digest
Ten micro liters of a mg/mL protein solution was dried down and resuspended in 8M urea, 100mM pH 8.5 Tris solution, 5mM DTT. The sample was heated at 60 degrees C for 1 hour and then diluted with 30uL of 100mM ammonium bicarbonate pH 8.0. Trysin was added at 1:100

trypsin to protein (w:w) and the sample was digested over night at 37 degrees C and stored at -80 degrees C until LC/MS/MS analysis.

Mass spectrometry

Digested protein samples were analyzed by LC/MS/MS (liquid chromatography mass spectrometry) methods for protein identification. Following protein digestion, samples were injected onto a reverse phase C18 column for separation of the injected peptides. Eluted LC peaks underwent MS/MS detection on a Qtof Premier mass spectrometer by Waters. A PLGS (Waters) search of the MS/MS data was performed using the NCBI protein database and this returned high confidence protein identifications.

Mice and viruses

The male wild type BALB/c mice were bred at Montana State University, Bozeman, MT. The influenza virus strains A/PR8/8/34 (PR8; H1N1) and A/HKx31 (X31; H3N2) were obtained from the Trudeau Institute, Saranac Lake, NY, USA. All studies described here were approved by the IACUC board at Montana State University or Utah State University prior to their performance.

Inoculation procedures and tissue recovery

Administration of the PCN and viral infections were carried out while mice were under a light anesthesia using 5% isoflurane inhalation. The PCN inoculations contained 100 mg per dose, the PR8 influenza inoculum contained 1500 PFU, Daily body weights of the mice were monitored following infection. At designated times following viral infection, mice were sacrificed by intraperitoneal administration of a lethal dose of sodium pentobarbital (90 mg/kg) followed by exsanguination when the mice no longer exhibited a pedal reflex. Lungs were then harvested, snap-frozen in liquid nitrogen and then stored at 280uC for future use in viral plaque assays. Lungs used for immuno-histological staining were instilled with O.C.T. Tissue Tek (Sakura Finetek USA Inc., Torrance CA, USA), snap frozen on liquid nitrogen and stored at 280uC for future use. Lung sections were cut and stained with FITC-conjugated antimouse B220, PE-conjugated anti-mouse CD4 or PE-conjugated anti-mouse CD21 (BD Biosciences San Diego CA, USA).

Recovery of broncho-alveolar lavage fluid

Broncho-alveolar lavage fluids (BALF) were obtained by washing the lungs with 2.0 ml of 3 mM EDTA in HBSS in two PCN Enhances Lung Immunity aliquots of 1 ml. Cells recovered in the BALF were counted and then spun out of the

recovered BALF. The recovered fluid was then stored at 280uC for future use in determining levels of serum albumin, lactate dehydrogenase, and influenza-specific antibody.

Determination of influenza-specific antibody levels

Determination of the PR8-specific antibody levels in the serum and BALF was carried out as described previously [18]. Briefly, 100 ul aliquots of a 1/100 dilution of serum or 100 ul aliquots of the BALF were added to 96-well high binding polystyrene ELISA plates that had already been coated with our PR8 influenza viral membrane preparation and subsequently blocked with 5% nonfat skim milk. The plates were allowed to incubate for 2 h at 37uC. Following 3 washes with PBS-Tween, 100 ul of a secondary alkaline phosphatase-conjugated anti-mouse isotype-specific antibody (Southern Biotechnology Associates, Birmingham AB) was added. The plates were then allowed to incubate for 2 h at 37uC. The presence of bound Ab was detected by the addition of pnitrophenyl phosphate in diethanolamine buffer and visualized at 405 nm.

Titration of viral recovery from lungs

Our previously described plaque assay procedure was used in the experiments reported here [19]. Briefly, serial 10-fold dilutions of the lung homogenates were used to inoculate confluent monolayers of Madin-Darby canine kidney cells. Following the inoculation procedure, the assay was then allowed to incubate at 35uC for 3–4 days prior to being fixed in 20% acetic acid and stained with 0.2% crystal violet to reveal the presence of viral plaques.